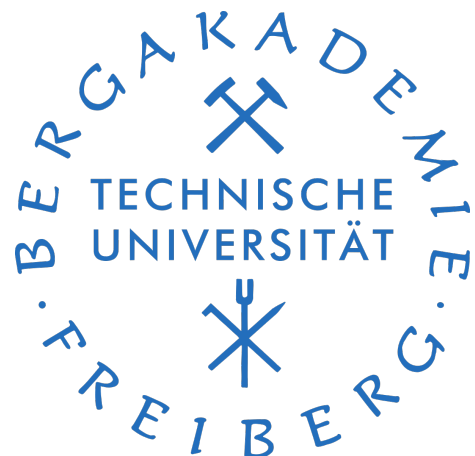


Development and implementation of material subroutines for fibre reinforced plastics in a commercial FEM software

Master thesis

Winter semester 2018/19



Presented by: Arun prakash Ganapathy

Supervised by: Dr.-Ing Dominik Laveuve

Mat.Nr: 63876

E-mail: arun-prakash.ganapathy@student.tu-freiberg.de

Contents

1	Introduction	1
1.1	Background and motivation	1
1.2	Scope and Outline	3
2	Continuum damage mechanics	6
2.1	Damage	6
2.2	Representative Volume Element(RVE)	7
2.3	Concept of continuum damage mechanics (CDM)	8
2.3.1	Modelling by Effective area reduction	8
2.3.2	Modelling by variation of elastic modulus	9
2.4	Mechanical representation of the damage state	10
2.4.1	Scalar damage variable	10
2.4.2	Vector damage variable	10
2.4.3	Damage tensor of second order	11
2.5	Effective Stress Tensors	11
2.5.1	Effective stress tensor for isotropic damage	12
2.5.2	Asymmetric effective stress tensor for anisotropic damage . . .	12
2.5.3	Symmetrized effective stress tensor for anisotropic damage (Murakami and Ohno 1981)	12
2.6	Damage effect tensors	12
2.7	Hypothesis of strain Equivalence	13
2.8	Hypothesis of strain energy equivalence	15
2.9	Elastic constitutive equation and elastic modulus tensor of orthotropic material	16
3	Working environment	19
3.1	Software tools required	19
3.2	Programming the UMAT	20
3.3	Compiling the UMAT	21
3.4	Creating FE model	22
3.5	Testing the UMAT	23
3.6	PostProcessing	24

4 Progressive failure analysis of orthotropic composite materials	26
4.1 Fibre-reinforced Composites	26
4.2 Mechanisms of damage and failure in fibre reinforced composites	26
4.2.1 Longitudinal failure	27
4.2.2 Transverse failure	27
4.3 Damage initiation criteria	28
4.3.1 3D Hashin's quadratic strain criteria	28
4.3.2 Maximum stress criteria	29
4.3.3 Modified Hashin's failure criterion	30
4.4 Types of damage evolution	30
4.4.1 Isotropic damage	31
4.4.2 Anisotropic damage	32
4.5 Localisation and Mesh Regularisation	33
4.6 Numerical implementation of the damage model in ANSYS	34
4.6.1 Strain based damage model	34
4.6.2 Stress based damage model	35
4.7 Schematic of UMAT implementation	37
5 Results and Discussion	38
5.1 Modelling linear elastic behaviour of orthotropic materials	38
5.2 Damage behaviour at integration point level	40
5.2.1 Uniaxial tension	41
5.2.2 Biaxial tension	46
5.2.3 Triaxial tension	47
5.3 Representative structural examples	48
5.3.1 Notched tensile specimen	50
5.3.2 Compact Tension (CT) Specimen	55
5.3.3 Plate with hole (3D)	63
6 Summary and Conclusion	68
A.1 Elastic stiffness matrix of the damaged material	IX
A.1.1 Plane stress (2D)	IX
A.1.2 3D	IX

List of Figures

1.1	Composite materials used in a Boeing 787 'Dreamliner'	1
1.2	Strain-softening of composite materials after damage initiation	2
2.1	Scales of damage observation	7
2.2	Effective area reduction due to microcracks	8
2.3	Damage of bar under tensile load	9
2.4	Surface element in RVE of a damaged material	11
2.5	Hypothesis of strain equivalence	14
2.6	Hypothesis of strain energy equivalence	15
3.1	Usermat Interface	21
3.2	Table (TB) commands	23
3.3	Time history post processor window	24
4.1	Fracture planes in FRP material	27
4.2	Types of degradation behaviour in damaged composite materials	31
5.1	Stress-Strain relation (Standard vs user-defined material routine)	38
5.2	Contour plots of the stress components σ_{11}, σ_{22} and σ_{33} of the bar obtained using standard (Figures a,c,e on the left) and user-defined material routine (Figures b, d, f on the right)	40
5.3	Evolution of stress for uniaxial tension test in 11 direction	41
5.4	Evolution of damage components for uniaxial tension test in 11 direction	42
5.5	Influence of softening parameter P in the damage evolution)	42
5.6	Convergence issue: Residual norm of the stress <i>vs</i> No of Newton-Raphson iterations	43
5.7	Evolution of stress and damage components with stress-based damage initiation criteria under uniaxial tension	44
5.8	Influence of element volume (V) on the damage evolution	45
5.9	The strain components ϵ_{22} and ϵ_{33} computed using algorithmic (a) and numerical tangent stiffness (b) under uniaxial tension	46
5.10	Evolution of stress (Figures a, c on the left) and corresponding damage (Figure b, d on the right) components under biaxial tension	47

5.11 Evolution of stress (Figures a, c, e on the left) and corresponding (Figures b ,d, f on the right) damage components under triaxial tension	48
5.12 Specimen geometry and boundary conditions. Dimensions are given in mm. Displacement controlled loading U_x is applied.	50
5.13 Considered meshes (h is the length of the element along fracture zone and n the total number of elements)	51
5.14 Convergence study: Global force-displacement response for model with regularization (Figure a on the left) and without regularization (Figure b the right)	51
5.15 Convergence study for model with(Figure a,c,e) and without(b,d,f) regularization: Damage contour plots d_1 at the end of the loading . .	53
5.16 Damage contour plots d_2 at the end of the loading (Loading in transverse direction)	54
5.17 Comparison of force-displacement response in longitudinal and transverse direction for h=0.5mm discretization	54
5.18 Specimen geometry and boundary conditions. Dimensions are given in mm. Displacement controlled loading U_x is applied	55
5.19 Considered meshes (h is the length of the element along fracture zone and n the total number of elements)	56
5.20 Convergence study: Global force-displacement response for three different meshes	57
5.21 Damage distributions at the end of loading in longitudinal direction: Damage contour plots d_1 and d_2	58
5.22 Damage distributions at the end of loading in transverse direction: Damage contour plots d_1 and d_2 (h = 1mm discretization)	58
5.23 Comparison of force-displacement response in longitudinal and transverse direction for h = 1 mm discretization	59
5.24 Comparison of force-displacement response for different shear co-efficient (α) (h= 1mm discretization)	59
5.25 Evolution of stress components during longitudinal tensile loading (h= 1mm discretization)	60
5.26 Damage distributions at the end of longitudinal loading: Damage contour plots d_2 for different shear co-efficients (α)	61
5.27 Evolution of stress components during transverse tensile loading (h= 1mm discretization)	62
5.28 Damage distributions at the end of transverse loading: Damage contour plots d_1 for different shear co-efficient (α)	62
5.29 Specimen geometry and boundary conditions. Dimensions are given in mm. Displacement controlled loading U_x is applied	63
5.30 Finite element discretization used for 3D damage study	64

5.31 Global force-displacement response for the longitudinal tensile loading	65
5.32 Contour plots of the damage distribution d_1 , d_2 and d_3 at the end of longitudinal tensile loading	67

List of Tables

4.1	Maximum stress criterion	29
5.1	Material parameters (Integration point studies)	39
5.2	Material parameters (Representative structural examples)	49
5.3	Material parameters (3D Damage model)	64

Chapter 1

Introduction

1.1 Background and motivation

Composite materials are made of two or more dissimilar materials of different physical or chemical properties, which, when combined, create a material with properties unlike the individual constituent materials. One of the earliest use of composite materials date back to 3400 B.C when Mesopotamians glued wood strips at different angles to create plywood. Now a days advanced composite materials are widely used in structural design in various industries such as aerospace, automobile, marine, petrochemical etc., due to their superior properties over traditional engineering materials.

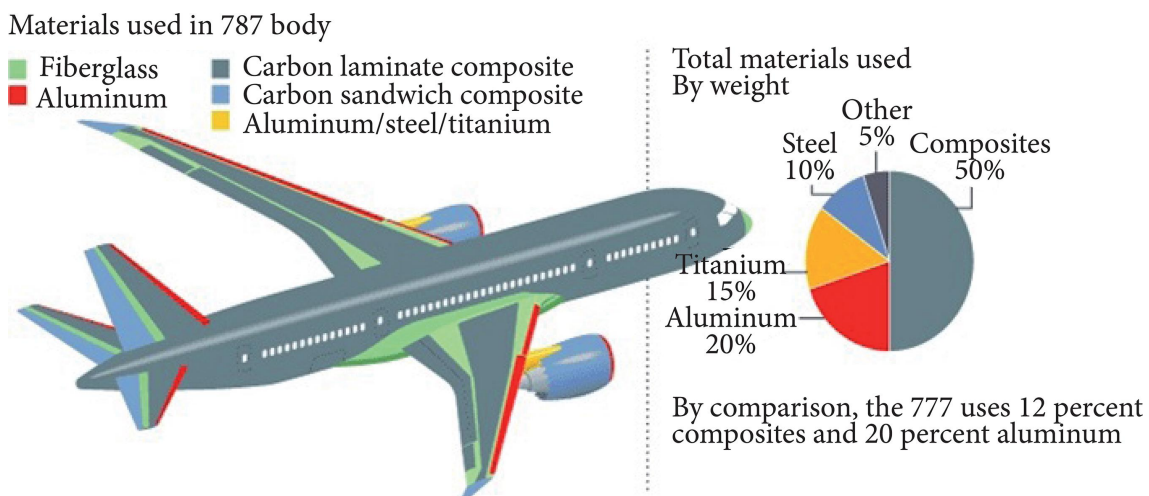


Figure 1.1: Composite materials used in a Boeing 787 'Dreamliner'

Composite materials are attractive because of their high strength, high stiffness-to-density ratio, light weight properties etc., Another important reason for using composite materials is the ability to tailor the stiffness and strength to specific

design loads flexibly. Despite their superior physical properties, composite materials can be damaged from a number of sources, both during initial processing and in operation. Since composite materials have complex material response and a negligible margin of safety through ductility as offered by metals, the development of damage must be understood for predicting failure of such materials. For example fibre-reinforced plastics exhibit local damage such as fibre breakage, matrix cracks, fibre matrix debonds etc., under normal operating conditions which may contribute to the failure. Therefore the ability to predict the initiation and growth of damage is important for predicting the performance, safety and reliability of the composite materials for commercial use.

Several methods have been proposed to analyze the failure of composite materials. The simplest of them is to degrade the stiffness of the material instantaneously using a degradation factor once the failure criteria is met. While easy to implement, the sudden complete failure of the material does not agree well with the real-life behaviour. Progressive failure analysis of composite materials is required to predict the real-life mechanical behaviour under various loading conditions. Over the last few decades continuum damage mechanics (CDM) first proposed by Kachanov (1987), has been employed to analyse the progressive degradation of the materials. The CDM approach provides a methodology which can determine the full range of deterioration of the material starting from no damage to the fully disintegrated material.

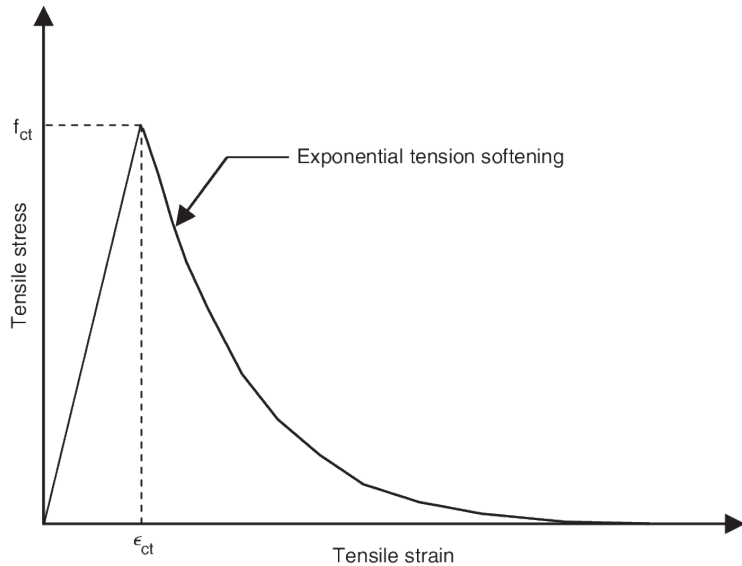


Figure 1.2: Strain-softening of composite materials after damage initiation

In CDM the damage is represented by a set of damage variables which describes the current state of the material, and their development using set of evolution laws. Once the failure criteria is met, the damage variables are calculated using these evolution laws and the stiffness of the material is degraded with the help of the damage

variables i.e., the material experiences strain-softening rather than strain-hardening observed in metals Figure (1.2). The very fact that the damage can be represented as a set of variables, makes them suitable for numerical simulations. Damage formulations can be easily fitted into non-linear finite element (FE) algorithms with the help of constitutive relations and implemented in simulation codes without the need to rely on special discretization techniques.

1.2 Scope and Outline

The objective of the thesis is to develop progressive damage models for predicting the initiation and propagation of damage in an orthotropic material when subjected to various loading conditions. Continuum damage mechanics (CDM) provides the framework for developing these damage models. Since the orthotropic materials exhibit different material properties in mutually perpendicular directions, the model essentially consists of linear elasticity extended with an anisotropic damage mechanism. Therefore one damage variable is assigned to each principal material direction to represent the development of damage i.e., 2 damage variables are required when the problem is in 2D/Plane-stress and 3 variables when the problem is in 3D. The numerical modelling of the strain-softening behaviour results in strong mesh dependency which results in convergence issues when the mesh is refined. To reduce the mesh sensitivity, the fracture energy approach is used which includes fracture energy in the damage evolution laws. This ensures the objectivity of the model by adjusting the energy dissipated by each failure mechanism using a characteristic element length.

The stages of the thesis work are briefly described as follows

Chapter 2 introduces the theoretical framework of continuum damage mechanics (CDM), constitutive relations and constitutive equations necessary for developing orthotropic material model.

Chapter 3 gives reader a brief introduction into software used and the instructions to develop, compile and implement a material model in an FE environment.

Chapter 4 gives a brief introduction to the mechanisms of damage and the different types of failure criteria and evolution equations necessary for developing damage models. In the end, the chapter deals with regularization method used to reduce mesh sensitivity problems and a brief description of how to implement the damage models step by step in a programming software.

Chapter 5 The results of the finite element simulations are discussed in this chapter. Starting with the implementation of linear elastic behaviour of the orthotropic

material the chapter discusses the behaviour of the damage models at integration point level and using representative structural examples.

Chapter 2

Continuum damage mechanics

Continuum damage mechanics (CDM) is a theory for analyzing damage and fracture processes in materials from a continuum mechanics point of view. (CDM) provides a continuum perspective for microflaws initiation, propagation, and their coalescence that eventually results in macroscopic faults and fractures. CDM uses state variables to represent the damage effect on the stiffness and remaining life of the material that is deteriorating as a result of load and ageing. A damage activation function is required to predict the initiation of damage. Damage evolution does not progress spontaneously after initiation therefore, a mathematical model is required.

2.1 Damage

Consider a body B of Fig. 2.1 where a crack of length a has developed due to an external load F . If we take an arbitrary point $P(x)$ near the crack tip, a number of microscopic cavities or microcracks would be observed around the region. These cavities are usually developed due to breakage of atomic bonds, or some defects in the atomic array. From the microscopic point of view, fracture of materials is a process of nucleation of microcavities or microcracks due to the breakage of atomic bonds. From the macroscopic point of view, it is a process of extension of cracks brought about by the coalescence of these microcracks.

From the mesoscopic point of view, which exists between microscopic and macroscopic scale, it is a process of nucleation, growth and the coalescence of microscopic cavities that leads to the initiation of macroscopic crack. The development of microscopic, mesoscopic and macroscopic processes of fracture in materials and the resulting deterioration in their mechanical properties is called damage. Continuum damage mechanics aims to analyse the damage development during mesoscopic and macroscopic fracture processes in the framework of continuum mechanics.

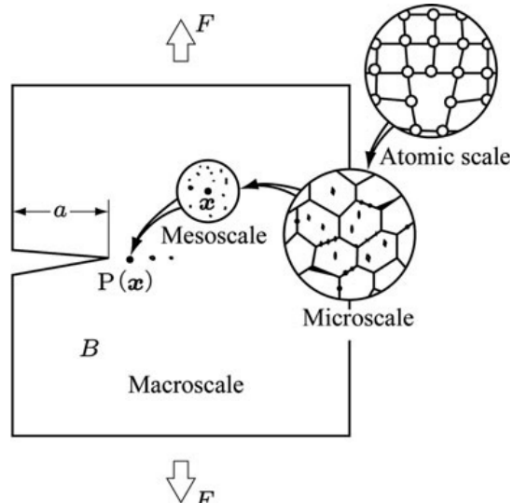


Figure 2.1: Scales of damage observation

2.2 Representative Volume Element(RVE)

To discuss the effects of microscopic discontinuities in a material using CDM we must homogenize the mechanical effects of microstructure and represent them as a macroscopic continuous field in the material. For this purpose, we take a small region of a mesoscale around the material point $P(x)$ in body B , as shown in Figure. 2.1. We assume that the material with discontinuous structures in this region as homogeneous, and the mechanical state of the material in this region can be represented by the statistical average of the mechanical variables in that region. This region is said to be the Representative Volume Element(RVE). For such RVE, the following two conditions must be satisfied:

- For the material in the RVE to be statistically homogeneous, the RVE should be large enough to contain a sufficient number of discontinuities
- To represent a non-uniform macroscopic mechanical field by means of a continuum, the size of RVE should be sufficiently small so that the variation of the macroscopic variable in it may be insignificantly small

The size of RVE depends on the microstructure of the relevant material and their typical sizes are as follows

- Metals and ceramics - 0.1 mm^3
- Polymers and composites - 1 mm^3
- Timber - 10 mm^3
- Concrete - 100 mm^3

2.3 Concept of continuum damage mechanics (CDM)

The basic concept of CDM is that a set of damage variables can represent the microstructural defects in a material. Continuum damage mechanics first represent the damage state of a material in terms of a set of internal state variables and then describe the mechanical behaviour of the damaged material and then development of damage by use of these state variables. The mechanical behaviour of a damaged material can be described using the notion of effective stress, together with the hypothesis of mechanical equivalence between damaged and undamaged material. The concept of effective stress and mechanical equivalence will be discussed in the following sections.

2.3.1 Modelling by Effective area reduction

Let us consider body B of Fig. (2.2) and take an RVE at an arbitrary point $P(x)$ in B . If the total void area in dA is dA_D , the mechanical effect of dA will be decreased by dA_D . Then the area,

$$d\tilde{A} = dA - dA_D \quad (2.1)$$

may be interpreted as the area which carries the internal force and is called an *effective area*. Thus, the damage variable D can be specified as

$$D = \frac{dA - d\tilde{A}}{dA} = \frac{dA_D}{dA} \quad (2.2)$$

where the damage variable D takes a value between 0 and 1 ($0 \leq D \leq 1$). $D = 0$ represents initial undamaged state and $D = 1$ represents fully damaged state.

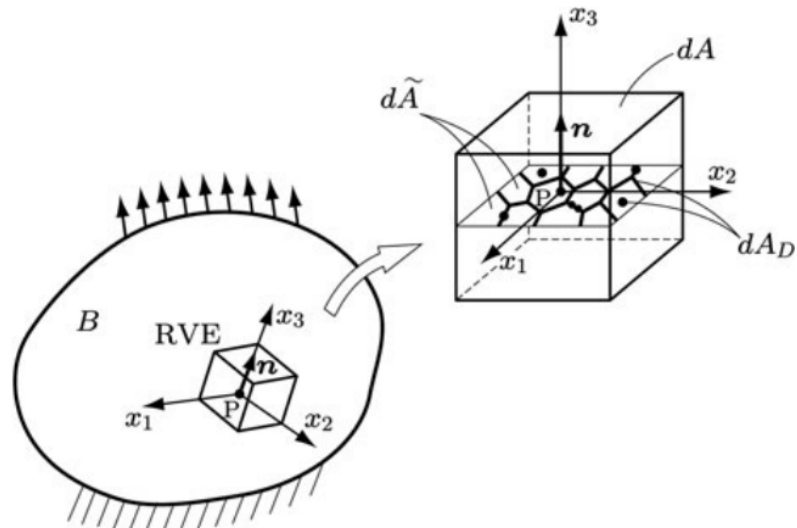


Figure 2.2: Effective area reduction due to microcracks

Suppose a cylindrical bar of cross-sectional area dA is subject to a tensile load dF , then the actual load carrying area is $d\tilde{A}$ rather than dA . According to eqns (2.1) and (2.2) the effective area $d\tilde{A}$ is given by,

$$d\tilde{A} = (1 - D)dA \quad (2.3)$$

The decrease in the load-carrying area increases the effect of stress σ induced by the external force dF . Due to eqn 2.3, the magnified stress $\tilde{\sigma}$ is given by,

$$\tilde{\sigma} = \frac{dF}{d\tilde{A}} = \frac{\sigma}{1 - D} \quad (2.4)$$

Since the stress $\tilde{\sigma}$ represents the stress magnified by the net area reduction due to damage, it is called *effective stress*. From eqn (2.3) and (2.4) we can postulate that the damaged cylindrical bar of Figure.(2.3b) with the cross-sectional area dA subject to force dF is mechanically equivalent to the fictitious undamaged bar of Figure.(2.3c), which is subject to force dF , has the cross-sectional area $d\tilde{A}$ and hence stress $\tilde{\sigma}$

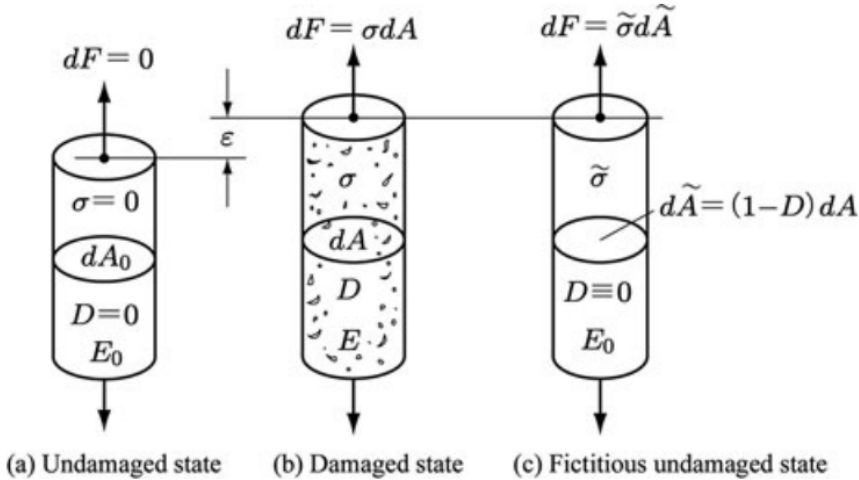


Figure 2.3: Damage of bar under tensile load

2.3.2 Modelling by variation of elastic modulus

Since the development of microcavities causes the reduction in material stiffness, the damage state can be characterized by variation in elastic modulus. Let us consider the bar (b) and (c) of Figure. (2.3) are in the damaged and fictitious undamaged state, respectively. Then the elastic strain ϵ in the bar (c) caused by stress $\tilde{\sigma}$ should be equal to the ϵ of the bar (b) under stress σ ; i.e.,

$$\tilde{\sigma} = E_0\epsilon, \quad \sigma = E(D)\epsilon \quad (2.5)$$

$$\epsilon = \frac{\sigma}{E(D)} = \frac{\tilde{\sigma}}{E_0} \quad (2.6)$$

where E_0 and $E(D)$ are the young's modulus of the material in the initial undamaged state and in damaged state after loading, respectively. Therefore, eqn. (2.6) defines another effective stress

$$\tilde{\sigma} = \frac{E_0}{E(D)} \sigma \quad (2.7)$$

By combining Eqn. (2.4) and (2.6) we get,

$$E(D) = (1 - D)E_0 \quad (2.8)$$

$$D = 1 - \frac{E(D)}{E_0} \quad (2.9)$$

Therefore, the damage variable D is characterized by the variation in Young's modulus $E(D)$. The modelling of damage by means of reduction in stiffness can be applied also to the anisotropic damage of brittle materials like composite materials, concrete, rocks etc.,

2.4 Mechanical representation of the damage state

The deformation of material depends on the direction of applied stress or strain, and hence it is an anisotropic phenomena. Therefore different theories have been developed for modelling 3-D anisotropic damage phenomenon. Some fundamental theories that describe 3-D damage state are given below.

2.4.1 Scalar damage variable

In the case of random or isotropic distribution of microcracks or voids, and when void density is small, the global mechanical properties can be approximated as nearly isotropic. The damage state, in this case, may be represented using scalar damage variable D . Thus isotropic damage theory based on isotropic damage variable has been often applied to 3-D problems of creep, elastic-plastic, ductile and fatigue damage

2.4.2 Vector damage variable

The damage state can be specified by the decrease in load carrying effective area due to void development. Hence it is easy to postulate a vector damage variable. Kachanov (1974, 1986) tried to extend the definition of damage to anisotropic damage by noting a surface element in an arbitrary direction n , he proposed vector damage variable $\omega = \omega_n n$, where ω_n is the effective area fraction.

2.4.3 Damage tensor of second order

To describe an anisotropic damage state, a damage variable of second or higher order tensor is required. Eqn.(2.3) suggests that the damage state (1 - D) is specified by the transformation of the surface element dA of Fig. (2.3b) of the damage state into the corresponding surface element $d\tilde{A}$ in the fictitious undamaged state of Fig.(2.3c). To express damage as a second order tensor, we first consider

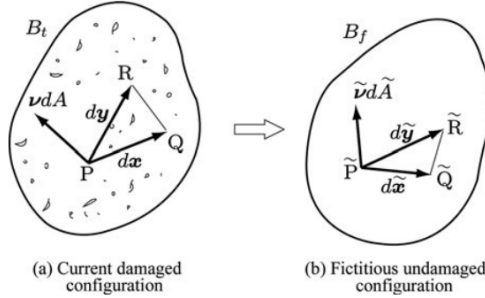


Figure 2.4: Surface element in RVE of a damaged material

an arbitrary surface element PQR in RVE in the current damaged configuration B_t of Fig.(2.4a). The unit normal vector and area of PQR are denoted by ν and dA . We further postulate the fictitious undamaged configuration B_f of Fig.(2.4b) mechanically equivalent to B_t , and the surface element and its area vector are denoted by $\tilde{P}\tilde{Q}\tilde{R}$ and $\tilde{\nu}d\tilde{A}$ respectively. According to Eqn.(2.3) the damage variable of second-order tensor D should be defined by linear transformation from area vector νdA in B_t into $\tilde{\nu}d\tilde{A}$ in B_f , i.e.,

$$\tilde{\nu}d\tilde{A} = (I - D)\nu dA \quad (2.10)$$

where I is the second order identity tensor. Since the damage tensor D is symmetric, it can be expressed by its spectral decomposition

$$D = \sum_{i=1}^3 D_i n_i \otimes D_i n_i \quad (2.11)$$

where D_i and n_i are the principal values and principal directions of D .

2.5 Effective Stress Tensors

The effective stresses are used to describe the mechanical behaviour of the damaged material. Some of the effective stresses postulated in damage mechanics are given below

2.5.1 Effective stress tensor for isotropic damage

If the damage state is isotropic then the effective stress tensor of three-dimensional state is given by

$$\tilde{\sigma} = (1 - D)^{-1} \sigma \quad (2.12)$$

where D is the scalar damage variable, and σ is the Cauchy stress tensor. This effective stress simplifies damage theory and can be applied to a number of damage problems like ductile damage. But this cannot be applied to damage of significant anisotropy, such as brittle damage due to microcrack distribution.

2.5.2 Asymmetric effective stress tensor for anisotropic damage

The increase in stress caused by the net area reduction in case of anisotropic damage is given by

$$\tilde{\sigma} = (I - D)^{-1} \sigma \quad (2.13)$$

where I and D are second-order identity tensor and the second-order damage tensor, respectively. In the actual development of anisotropic damage, the stress-induced in the RVE of damage material is asymmetric. But asymmetric stress tensors make the numerical analysis complicated, and thus different methods of symmetrization have been proposed. A few of them are described as follows

2.5.3 Symmetrized effective stress tensor for anisotropic damage (Murakami and Ohno 1981)

A simple symmetrization procedure of Eq.(2.14), the symmetric part of the Cartesian decomposition of Eq.(2.14) gives,

$$\tilde{\sigma} = \frac{1}{2}[(I - D)^{-1} \sigma + \sigma(I - D)^{-1}] \quad (2.14)$$

2.6 Damage effect tensors

The general form of an effective stress tensor $\tilde{\sigma}$ is given by the damage effect tensor \mathbb{M} and the corresponding Cauchy stress tensor σ , i.e.,

$$\tilde{\sigma} = \mathbb{M} : \sigma \quad (2.15)$$

It is convenient to express the tensors in the form of matrices and then execute the tensor operations as a matrix calculus.. To simplify this procedure, we take an orthonormal basis n_i with principal directions n_i of the second-order symmetric damage tensor D , and represent the tensor in terms of its component to this basis. According to Voigt notation, the second-order symmetric tensor σ and the related effective stress $\tilde{\sigma}$ are expressed by the column vector of six dimensions:

$$[\sigma_P] \equiv [\sigma_{11} \ \sigma_{22} \ \sigma_{33} \ \sigma_{12} \ \sigma_{13} \ \sigma_{23}]^T \quad (2.16)$$

$$[\tilde{\sigma}_P] \equiv [\tilde{\sigma}_{11} \ \tilde{\sigma}_{22} \ \tilde{\sigma}_{33} \ \tilde{\sigma}_{12} \ \tilde{\sigma}_{13} \ \tilde{\sigma}_{23}]^T \quad (2.17)$$

By means of the matrix representation, we have the matrix form

$$[\tilde{\sigma}_P] \equiv [\mathbb{M}_{pq}] : [\sigma_P] \quad (2.18)$$

Matrix representation of the damage effect tensor of Eq.(2.18) is shown below

$$[\mathbb{M}_{pq}] \equiv \begin{bmatrix} \frac{1}{\omega_{11}} & 0 & 0 & 0 & 0 & 0 \\ 0 & \frac{1}{\omega_{22}} & 0 & 0 & 0 & 0 \\ 0 & 0 & \frac{1}{\omega_{33}} & 0 & 0 & 0 \\ 0 & 0 & 0 & \frac{1}{\omega_{12}} & 0 & 0 \\ 0 & 0 & 0 & 0 & \frac{1}{\omega_{23}} & 0 \\ 0 & 0 & 0 & 0 & 0 & \frac{1}{\omega_{13}} \end{bmatrix}$$

where

$$\omega_{11} = (1 - d_1) \quad \omega_{22} = (1 - d_2) \quad \omega_{33} = (1 - d_3)$$

$$\omega_{12} = \sqrt{(1 - d_1)(1 - d_2)} \quad \omega_{23} = \sqrt{(1 - d_2)(1 - d_3)} \quad \omega_{13} = \sqrt{(1 - d_1)(1 - d_3)}$$

2.7 Hypothesis of strain Equivalence

The inelastic constitutive equation of a damaged material is given by the corresponding constitutive equation for an undamaged material by replacing the stress tensor σ in the equation with the corresponding effective stress tensor $\tilde{\sigma}$. In Figure (2.5). the effect of stress σ acting on RVE in the current damaged configuration B_t is equivalent to that of the stress $\tilde{\sigma}$ in the fictitious undamaged configuration.

Therefore the deformation of the damaged material subject to stress σ should be equal to that of the fictitious undamaged material subject to stress $\tilde{\sigma}$. Suppose the constitutive equation of an undamaged inelastic material is given by

$$\epsilon = F_0(\sigma, \alpha) \quad (2.19)$$

or

$$\dot{\epsilon} = F_0(\sigma, \alpha) \quad (2.20)$$

where α is an internal variable representing the internal change other than damage. and (\cdot) denotes the material time derivative Then according to hypothesis of

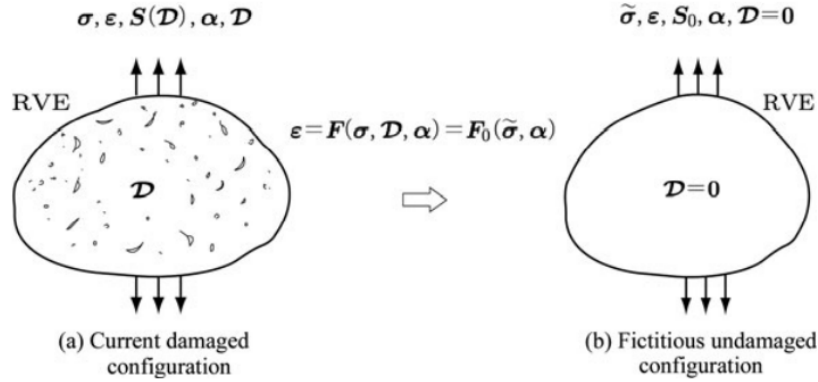


Figure 2.5: Hypothesis of strain equivalence

strain equivalence, the inelastic constitutive equation of the damaged material represented by a damage variable D should be given by replacing σ of Eq.(25) with the effective stress $\tilde{\sigma}$ i.e.,

$$\epsilon = F(\sigma, D, \alpha) = F_0(\tilde{\sigma}, \alpha) \quad (2.21)$$

or

$$\dot{\epsilon} = F(\sigma, D, \alpha) = F_0(\tilde{\sigma}, \alpha) \quad (2.22)$$

In case of elastic deformation, constitutive equations for an undamaged and damaged material are given by

$$\epsilon = \mathbb{S}_0 : \sigma, \quad (2.23)$$

$$\epsilon = \mathbb{S}(D) : \sigma, \quad (2.24)$$

where \mathbb{S}_0 and $\mathbb{S}(D)$ are fourth-order elastic compliance tensors of the materials. Therefore, according to the hypothesis of strain equivalence the elastic constitutive equation of the damaged material and the compliance tensor are given by

$$\epsilon = \mathbb{S}_0 : \tilde{\sigma} = [\mathbb{S}_0 : \mathbb{M}(D)] : \sigma = \mathbb{S}(D) : \sigma \quad (2.25)$$

$$\mathbb{S}(D) = \mathbb{S}_0 : \mathbb{M}(D) \quad (2.26)$$

where $\mathbb{M}(D)$ is the damage effect tensor which is given by

$$\mathbb{M}(D) = \mathbb{S}_0^{-1} : \mathbb{S}(D) \quad (2.27)$$

2.8 Hypothesis of strain energy equivalence

The existence of a strain energy function necessitates the symmetry of the compliance and elastic modulus tensor. But the compliance tensor resulting from the hypothesis of strain equivalence is asymmetric which does not satisfy the requirement. Therefore the hypothesis of strain energy equivalence is used to satisfy the symmetry requirements. Let us consider an elastic-plastic material and represent the internal change due to plastic deformation by an internal state variable α . The complementary strain energy functions of the material at undamaged and damaged state are given, respectively as follows

$$V_0(\sigma, \alpha) = \frac{1}{2}\sigma : \mathbb{S}_0 : \sigma - \phi(\alpha) \quad (2.28)$$

$$V(\sigma, D, \alpha) = \frac{1}{2}\sigma : \mathbb{S}(D) : \sigma - \phi(\alpha) \quad (2.29)$$

Thus the constitutive equation for the undamaged and damaged material is

$$\epsilon = \frac{\partial V_0}{\partial \sigma} = \mathbb{S}_0 : \sigma \quad (2.30)$$

$$\epsilon = \frac{\partial V}{\partial \sigma} = \mathbb{S}(D) : \sigma \quad (2.31)$$

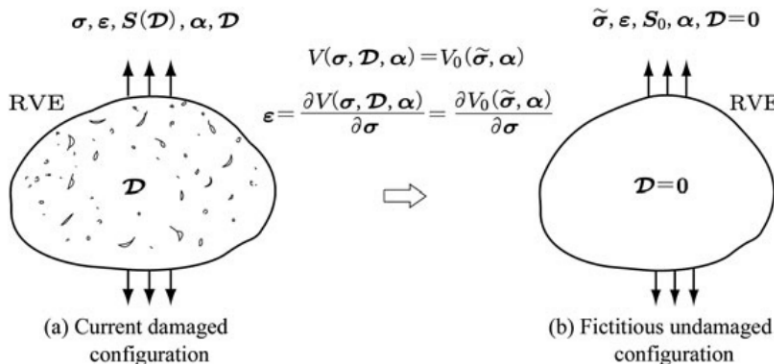


Figure 2.6: Hypothesis of strain energy equivalence

Suppose a damaged material of Figure.(2.6)a subject to stress σ , and represent the damage and internal state due to inelastic deformation by D and α , respectively. Then the strain energy function $V(\sigma, D, \alpha)$ of the damaged material is given by replacing σ in the corresponding function $V_0(\sigma, \alpha)$ of the undamaged material of Fig.(2.6)b with the effective stress $\tilde{\sigma}$

$$V(\sigma, D, \alpha) = V_0(\tilde{\sigma}, \alpha)$$

By the use of this hypothesis, the elastic strain of Eq.(2.31) leads to

$$\begin{aligned} \epsilon &= \frac{\partial V(\sigma, D, \alpha)}{\partial \sigma} = \mathbb{S}(D) : \sigma \\ &= \frac{\partial V_0(\tilde{\sigma}, \alpha)}{\partial \sigma} = \frac{\partial}{\partial \sigma} \left(\frac{1}{2} \tilde{\sigma} : \mathbb{S}_0 : \tilde{\sigma} \right) \\ &= \frac{1}{2} \frac{\partial}{\partial \sigma} [(\mathbb{M}(D) : \sigma) : \mathbb{S}_0 : (\mathbb{M}(D) : \sigma)] \\ &= [\mathbb{M}^T(D) : \mathbb{S}_0 : \mathbb{M}(D)] \end{aligned} \quad (2.32)$$

From Eq.(2.32), the elastic compliance tensor of the damaged material is given as follows

$$\mathbb{S}(D) = \mathbb{M}^T(D) : \mathbb{S}_0 : \mathbb{M}(D) \quad (2.33)$$

If the damage effect tensor $\mathbb{M}(D)$ can be expressed as a fourth-order symmetric tensor, then the elastic compliance tensor $\mathbb{S}(D)$ becomes a fourth-order symmetric tensor which satisfies the thermodynamic requirement.

2.9 Elastic constitutive equation and elastic modulus tensor of orthotropic material

Orthotropic materials are materials that exhibit different material properties along three mutually orthogonal axes. They are a special form of anisotropic materials because their properties change when measured from different directions. Some examples of orthotropic materials are wood, composite materials etc., Orthotropic materials require 9 independent variables to express their constitutive matrix. The 9 elastic constants are three Young's moduli E_x, E_y, E_z , the three Poisson's ratios

$\nu_{xy}, \nu_{yz}, \nu_{zx}$, and three shear moduli G_{xy}, G_{yz}, G_{zx} . The elastic stiffness matrix of orthotropic material has the form,

$$\sigma = \mathbb{C}_0 : \epsilon \quad \text{or} \quad \sigma_{ij} = C_{ijkl}^0 \epsilon_{kl}, \quad (2.34)$$

$$[C_{pq}^0] = \begin{bmatrix} \frac{1 - \nu_{yz}\nu_{zy}}{E_y E_z \Delta} & \frac{\nu_{xy} + \nu_{xz}\nu_{zy}}{E_y E_z \Delta} & \frac{\nu_{xz} + \nu_{xy}\nu_{yz}}{E_y E_z \Delta} & 0 & 0 & 0 \\ \frac{\nu_{yx} + \nu_{yz}\nu_{zx}}{E_x E_z \Delta} & \frac{1 - \nu_{xz}\nu_{zx}}{E_1 E_z \Delta} & \frac{\nu_{yz} + \nu_{yx}\nu_{xz}}{E_1 E_z \Delta} & 0 & 0 & 0 \\ \frac{\nu_{zx} + \nu_{yx}\nu_{zy}}{E_x E_y \Delta} & \frac{\nu_{zy} + \nu_{xy}\nu_{zx}}{E_x E_y \Delta} & \frac{1 - \nu_{xy}\nu_{yx}}{E_x E_y \Delta} & 0 & 0 & 0 \\ 0 & 0 & 0 & G_{xy} & 0 & 0 \\ 0 & 0 & 0 & 0 & G_{yz} & 0 \\ 0 & 0 & 0 & 0 & 0 & G_{zx} \end{bmatrix}$$

where

$$\Delta = (1 - \nu_{xy}\nu_{yx} - \nu_{yz}\nu_{zy} - \nu_{zx}\nu_{xz} - 2\nu_{xy}\nu_{yz}\nu_{zx}) / E_x E_y E_z$$

$$\text{and } \frac{\nu_{xy}}{E_y} = \frac{\nu_{yx}}{E_x}, \frac{\nu_{yz}}{E_z} = \frac{\nu_{zy}}{E_y}, \frac{\nu_{xz}}{E_z} = \frac{\nu_{zx}}{E_x}$$

Chapter 3

Working environment

The material models necessary for simulating progressive damage must be programmed first using a programming language, compiled, and then tested in a commercial FEM software. The programming language of choice for most commercial FEM software is FORTRAN because it is fast and straightforward. To program the material model, an integrated development environment (IDE) and a compiler compatible with the version of the FEM software are required. This chapter describes the necessary tools for creating material models and how to use them to test the models in detail.

3.1 Software tools required

- **OCTAVE**

Octave is an open-source version of programming language software MATLAB. Initially, the user material subroutines are developed on Octave and tested using simple tests like uniaxial tension with the help of constitutive driver routines

- **Visual Studio**

Visual Studio is the IDE used for programming and debugging user material subroutines using the FORTRAN programming language.

- **Intel parallel studio**

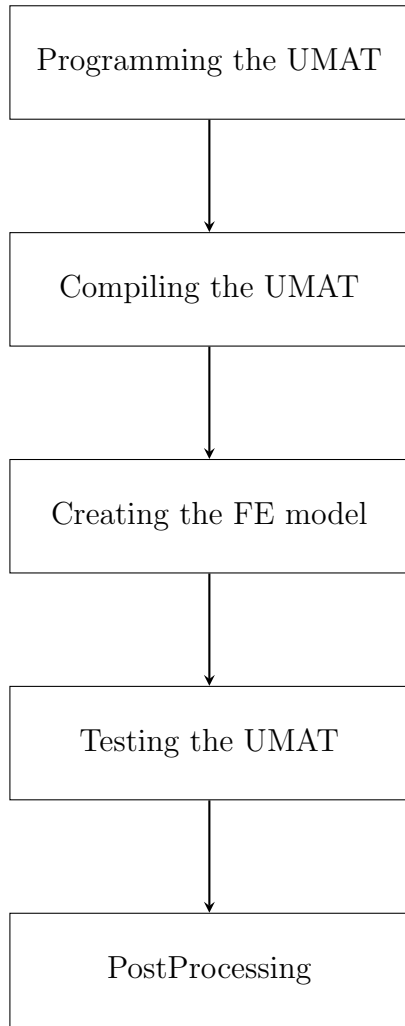
The compiler available in Intel parallel studio is used for compiling the material subroutines before testing them in a FEM software.

- **ANSYS**

ANSYS is the commercial FEM software chosen for creating models

of specimens and analyzing how the material models behave in different test conditions.

The following sections provide the reader with a detailed description, starting from developing the user-defined material subroutine to implementing and analysing the results in the ANSYS environment. The flowchart below shows the steps involved in the whole process



3.2 Programming the UMAT

The user material subroutine is an ANSYS programmable feature which allows users to write their own material constitutive equations within a newly developed general material framework. The subroutine is called at all material integration points of the element during the solution phase.

ANSYS demands the necessary variables declared in a certain way so that the USERMAT developed can work compatibly with ANSYS when it is called at

each integration point. The guidelines for declaring input and output arguments can be found on ANSYS' usermat guide. The following image shows the user subroutine interface with the set of possible input arguments that USERMAT can access from ANSYS

For every Newton raphson iteration, the USERMAT is called at every material

```

subroutine usermat(
& matId, elemId,kDomIntPt, kLayer, kSectPt,
& ldstep, isubst, keycut,
& nDirect, nShear, ncomp, nStatev, nProp,
& Time, dTime, Temp, dTemp,
& stress, statev, dsdePl, sedEl, sedPl, epseq,
& Strain, dStrain, epsPl, prop, coords,
& tsstif, epsZZ,
& var1, var2, var3, var4, var5,
& var6, var7, var8)

INTEGER
& matId, elemId,
& kDomIntPt, kLayer, kSectPt,
& ldstep, isubst, keycut,
& nDirect, nShear, ncomp, nStatev, nProp
DOUBLE PRECISION
& Time, dTime, Temp, dTemp,
& sedEl, sedPl, epseq, epsZZ
DOUBLE PRECISION
& stress (ncomp ), statev (nStatev),
& dsdePl (ncomp,ncomp),
& Strain (ncomp ), dStrain (ncomp ),
& epsPl (ncomp ), prop (nProp ),
& coords (3), rotateM (3,3),
& defGrad_t(3,3), defGrad(3,3),
& tsstif (2)

```

Figure 3.1: Usermat Interface

integration point, and ANSYS passes in strains, stresses and state variables at the beginning of the time increment and the current strain increment. The USERMAT then has to compute and update the necessary output arguments like stresses and state variables at the end of the increment and the material tangent stiffness matrix $\frac{\partial\sigma}{\partial\epsilon}$.

3.3 Compiling the UMAT

The user-programmable subroutines must be compiled before testing them in ANSYS environment. The compilation process first checks for errors in the source code and then converts it into ANSYS executable files (.dll files), which can be used by ANSYS. The compiler present in Intel parallel studio is used for this purpose. The step by step process of compiling the UMAT is given below

- Create an empty directory and copy the usermat file you want to compile (.f files) into the empty directory.
- Change the name of your usermat file to *usermat*

- Go to ”Control Panel>Search System>Edit the system environment variables>Environment variables” and click New in the user variables for your PC, which opens a window
- In that window, type ANS_USER_PATH for variable name and for variable value, copy and paste the path to your working directory and click Ok
- Go to folder ”C:\ Program Files\ ANSYS Inc\ v181\ ansys\ custom\ user\ win64” and copy the ANSUSERSHARED.bat file and paste it in the working directory
- Open command prompt and navigate to the working directory
- Type ANSUSERSHARED.bat and press enter. This opens the Intel compiler and asks for user-programmable feature source file name
- Type *usermat* without extension and press Enter.
- If there is no error in the *usermat* file the compiler will show the message ”usermatLib.dll has been successfully build.”
- For ANSYS to access these .dll files, open ANSYS Mechanical APDL product launcher and in the file management section browse to the current working directory
- Click run and in the Mechanical APDL output window you should see the message ”Note - This ANSYS version was linked by Licensee”. This indicates that you are using the shared library with the USERMAT

3.4 Creating FE model

The preprocessor section of ANSYS mechanical APDL is used to create and mesh the FE model. The ANSYS user-programmable feature can be used with 18x family elements, which include LINK180, PLANE 182, PLANE 183, SOLID 185, SOLID 186. The type of element required for creating FE models based on the problem can be chosen from the element type menu in the preprocessor section. Once the element type is chosen, the material model, and the material properties can be entered in the *Material props* section. The *Modelling* section can be utilised to create the geometry required for testing the subroutines and then can be meshed using the *Meshing* option.

To use the FE model, again and again, to test different material models with different material properties the FE model can be saved in the form of an APDL script. An APDL script is a simple text file containing the commands required to

create and solve the FE model. A simple way to create an APDL script for an FE model is to copy the log of commands automatically created in the log file during the creation of your model and pasting it to a new text file. This log file can be accessed by going to *List > Files > Logfile*. The created APDL script can then be accessed by going to *File > Read input from* and navigate and select your file.

3.5 Testing the UMAT

To use the user material option, the TB,USER command must be included in the APDL script so that the user material can be defined. The table command for USER material option is

TB,USER,matId,NTEMPS,NPTS

matId - material reference number

NTEMPS - Number of temperature points

NPTS - Number of material constants at a given temperature

If state variables are used in the subroutine, the number of state variables need to be defined in the APDL script by the command TB,STATE

TB,STATE,matId,,NPTS

matId - material reference number

NPTS - Number of state variables to be used in USERMAT

A simple example for defining a user material and two state variables is given in the Figure.(3.2) below

```
!*
YOUNG = 210e3
POISSON = 0.33
T1 = 1

TB,USER,1,1,2,
TBTEMP,T1
TBDATA,,YOUNG,POISSON
TB,STATE,1,,2
```

Figure 3.2: Table (TB) commands

Before defining boundary conditions (BCs), the entities required for solving the FE model, such as time at the end of the load step, the number of steps, the results to be stored etc., must be defined. This can be done using *Sol'n Controls* option in the solution menu. Once the BCs are defined, the model can be solved by giving the command *SOLVE*.

3.6 PostProcessing

Once the FE model has finished solving, the results can be analyzed using the 'General Postprocessor' option. The nodal and elemental solution for components like stress, strain, displacement etc., can be plotted using the 'contour plot' option, which can be found on Plot results. By default, this option plots the results at the last substep, so to plot the solution at the substep of one's choice one must navigate to *Read results > By pick* and select the substep to be plotted. Since the posprocessor of ANSYS does not have GUI option for plotting state variables the following command must be given: *plnsol, svar, n* where *n* is the number of the state variable to be plotted. The time history of a certain variable, such as stress, reaction force, strain etc., at a node or an element can be plotted using *TimeHist Postpro* option. On clicking the *TimeHist Postpro* option a *Variable List* window opens up. To add the variables to plot, click the green add symbol on the top-left corner which opens a window with the list of variables that can be added to the *Variable List* window. Once the variables have been added, the variables can be plotted against each other or against time. Fig.(3.3) shows the *Variable List* window with X-component of force and displacement of node 3 selected and plotted against each other.

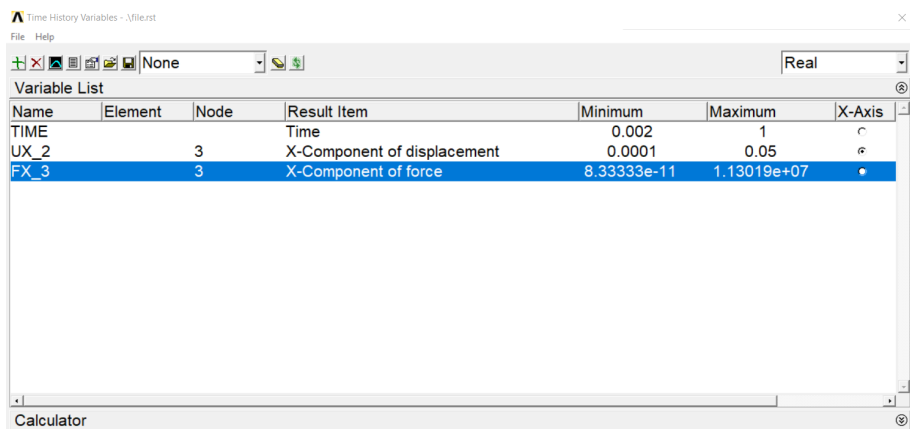


Figure 3.3: Time history post processor window

The time history results of each variable at a node or an element can also be saved as a text file using *List Data* option in the *Variable List* window.

Chapter 4

Progressive failure analysis of orthotropic composite materials

4.1 Fibre-reinforced Composites

Fibre-reinforced plastic composites is a term for a large family of materials ranging from short fibre reinforced polyamides to unidirectional graphite fibre epoxies. Fibre-reinforced composites consist of three components 1) the fibres as the discontinuous or dispersed phase, 2) the matrix as the continuous phase, and 3) the fine interphase region, also known as the interface. The first fibres used in fibre reinforced plastics are made of glass. Although the virgin strength of the glass is high, the actual strength is limited by the microscopic defects on the surface of the fibre. The graphite fibres are anisotropic due to their laminar structure. Graphite fibres maintain their strength even at high temperatures. Two types of plastics are commonly used as matrix materials, namely unsaturated polyesters and epoxies. The use of unsaturated polyesters is restricted to temperatures up to 100C. The main advantage of this material is the high amount of shrinkage at hardening, which causes high internal stress and decrease the strength of the material. The characteristics of epoxy are better than polyester resins. The material can withstand temperatures up to 250C and shrinks only 2% at hardening. However, epoxy resins are high in price compared to polyesters.

4.2 Mechanisms of damage and failure in fibre reinforced composites

The failure in fibre reinforced composites happens mainly due to matrix cracking or fibre failure. Therefore the failure can be divided mainly two types, namely 1) Longitudinal failure and 2) Transverse failure. The mechanism of both failure

mechanisms, their causes and their effects on material behaviour are discussed in detail below

4.2.1 Longitudinal failure

In fibre-reinforced plastics, the most significant portion of the load is carried by fibres. When the fibres fail, the load must redistribute to other areas of the structure and may cause structural collapse. Longitudinal tensile failure occurs in both constituents, and a fracture occurs along a plane whose normal is parallel to the fibre direction. Simple maximum stress or maximum strain can usually provide an accurate measure of longitudinal tensile failure. Longitudinal compressive failure occurs from the collapse of the fibres due to shear kinking and damage of the supporting matrix. Fibre misalignment causes shear stress between fibres that rotate fibres, which increases shear stress further and leads to instability.

4.2.2 Transverse failure

Transverse failure happens due to matrix cracking and fibre-matrix debonding. Under the presence of in-plane shear stress and transverse tensile stress, the combined effects of defects such as resin-rich regions, fibre-resin debonds, and resin voids trigger a transverse crack that extends through the thickness. The transverse cracks are formed at the fibre-resin interface without affecting the fibres. When a unidirectional fibre composite is loaded in shear, a non-linear shear stress-strain behaviour is observed before the material fails by through-thickness matrix cracking. This non-linear behaviour is due to the visco-plastic behaviour of the matrix and from the nucleation of microvoids.

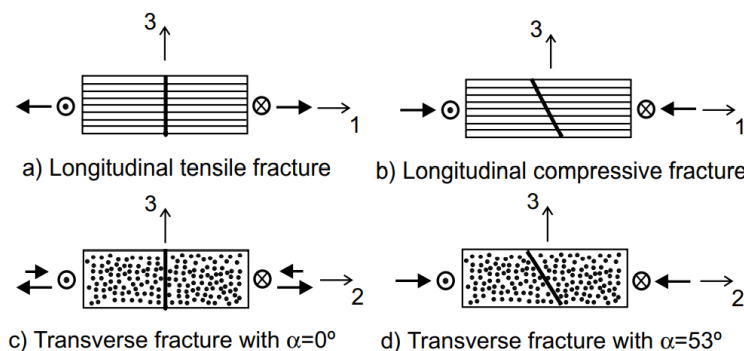


Figure 4.1: Fracture planes in FRP material

Experimental results have shown that moderate compression has beneficial effects on the strength of the material (Soden et al., 1998); when the transverse compressive stress value is smaller than the in-plane shear stress, the fracture plane is

perpendicular to the mid-plane of the ply. Increasing the compressive stress changes the angle of the fracture plane. For glass-epoxy and carbon-epoxy composites, when loaded in pure transverse compression, the fracture plane is at an angle of $53^\circ \pm 3^\circ$ with respect to the thickness direction. Therefore, the matrix cracking does not occur in the plane of maximum transverse shear stress (45°).

4.3 Damage initiation criteria

Damage initiation criteria refer to the onset of damage at a material point. Since the properties of orthotropic materials are different in the mutually perpendicular directions, three failure mode indices, F_f, F_m, F_z , are used for failure modes in three principal material directions. Since the failure due to tension and compression in each direction cannot happen at the same integration point and at the same time, the failure mode index must be calculated based on whether the material direction is under tension or compression. Some of the damage initiation criteria are given as follows

4.3.1 3D Hashin's quadratic strain criteria

Hashin's quadratic strain criteria includes shear strain components in addition to the normal strain components. The criteria for each material direction is given below

i) Longitudinal direction 1 ,

$$F_f^2 = \begin{cases} \left(\frac{\epsilon_{11}}{\epsilon_{11}^{f,t}}\right)^2 + \left(\frac{\epsilon_{12}}{\epsilon_{12}^f}\right)^2 + \left(\frac{\epsilon_{13}}{\epsilon_{13}^f}\right)^2 \geq 1 & (\epsilon_{11} > 0) \\ \left(\frac{\epsilon_{11}}{\epsilon_{11}^{f,c}}\right)^2 \geq 1 & (\epsilon_{11} < 0) \end{cases} \quad (4.1)$$

ii) Transverse direction 2,

$$F_m^2 = \begin{cases} \frac{(\epsilon_{22}+\epsilon_{33})^2}{\epsilon_{22}^{f,t} \epsilon_{33}^{f,t}} - \frac{\epsilon_{22}\epsilon_{33}}{(\epsilon_{23}^f)^2} + \left(\frac{\epsilon_{12}}{\epsilon_{12}^f}\right)^2 + \left(\frac{\epsilon_{13}}{\epsilon_{13}^f}\right)^2 + \left(\frac{\epsilon_{23}}{\epsilon_{23}^f}\right)^2 \geq 1 & (\epsilon_{22} > 0) \\ \frac{(\epsilon_{22}+\epsilon_{33})^2}{\epsilon_{22}^{f,c} \epsilon_{33}^{f,c}} + \frac{\epsilon_{22}+\epsilon_{33}}{\epsilon_{22}^{f,c}} \left(\frac{\epsilon_{22}^{f,c}}{2\epsilon_{12}^f} - 1 \right) - \frac{\epsilon_{22}\epsilon_{33}}{(\epsilon_{23}^f)^2} + \left(\frac{\epsilon_{12}}{\epsilon_{12}^f}\right)^2 \\ + \left(\frac{\epsilon_{13}}{\epsilon_{13}^f}\right)^2 + \left(\frac{\epsilon_{23}}{\epsilon_{23}^f}\right)^2 \geq 1 & (\epsilon_{22} < 0) \end{cases} \quad (4.2)$$

iii) Transverse direction 3,

$$F_z^2 = \begin{cases} \left(\frac{\epsilon_{33}}{\epsilon_{33}^{f,t}} \right)^2 + \left(\frac{\epsilon_{13}}{\epsilon_{13}^f} \right)^2 + \left(\frac{\epsilon_{23}}{\epsilon_{23}^f} \right)^2 \geq 1 & (\epsilon_{33} > 0) \\ \left(\frac{\epsilon_{33}}{\epsilon_{33}^{f,c}} \right)^2 + \left(\frac{\epsilon_{13}}{\epsilon_{13}^f} \right)^2 + \left(\frac{\epsilon_{23}}{\epsilon_{23}^f} \right)^2 \geq 1 & (\epsilon_{33} > 0) \end{cases} \quad (4.3)$$

in which $\epsilon_{ii}^{f,t} = \frac{\sigma_i^{f,t}}{C_{ii}}$, $\epsilon_{ii}^{f,c} = \frac{\sigma_i^{f,c}}{C_{ii}}$ ($i = 1, 2, 3$), $\epsilon_{12}^f = \frac{\sigma_{12}^f}{C_{44}}$, $\epsilon_{13}^f = \frac{\sigma_{13}^f}{C_{55}}$, $\epsilon_{23}^f = \frac{\sigma_{23}^f}{C_{66}}$

4.3.2 Maximum stress criteria

Since the load-carrying area decreases due to an increase in damage, the effect of stress gets magnified in the damaged material. Therefore, in the case of maximum stress criteria, normal stress components of the effective stress ($\tilde{\sigma}$) are checked against the failure strength in each principal material direction. The effective stress can be computed using the eqn.(2.15). The maximum stress criteria for each material direction are given in the table below

Damage direction	Tension	Compression
Longitudinal direction 1 (F_f)	$\frac{\tilde{\sigma}_{11}}{X_T} \leq 1$	$\frac{\tilde{\sigma}_{11}}{-X_C} \leq 1$
Transverse direction 2 (F_m)	$\frac{\tilde{\sigma}_{22}}{Y_T} \leq 1$	$\frac{\tilde{\sigma}_{22}}{-Y_C} \leq 1$
Transverse direction 3 (F_z)	$\frac{\tilde{\sigma}_{33}}{Z_T} \leq 1$	$\frac{\tilde{\sigma}_{33}}{-Z_C} \leq 1$

Table 4.1: Maximum stress criterion

where X_T, Y_T and Z_T are failure strength in tension and X_C, Y_C and Z_C are failure strength in compression in each principal material direction respectively.

4.3.3 Modified Hashin's failure criterion

Modified Hashin's failure criterion for plane stress condition is given below

i) Longitudinal direction 1,

$$F_f = \begin{cases} \left[\left(\frac{\tilde{\sigma}_{11}}{X_T} \right)^2 + \alpha \cdot \left(\frac{\tilde{\sigma}_{12}}{S} \right)^2 \right]^{\frac{1}{2}} \geq 1 & (\tilde{\sigma}_{11} > 0) \\ \left[\left(\frac{\tilde{\sigma}_{11}}{X_C} \right)^2 + \alpha \cdot \left(\frac{\tilde{\sigma}_{12}}{S} \right)^2 \right]^{\frac{1}{2}} \geq 1 & (\tilde{\sigma}_{11} < 0) \end{cases} \quad (4.4)$$

i) Transverse direction 2,

$$F_f = \begin{cases} \left[\left(\frac{\tilde{\sigma}_{22}}{Y_T} \right)^2 + \alpha \cdot \left(\frac{\tilde{\sigma}_{12}}{S} \right)^2 \right]^{\frac{1}{2}} \geq 1 & (\tilde{\sigma}_{22} > 0) \\ \left[\left(\frac{\tilde{\sigma}_{22}}{Y_C} \right)^2 + \alpha \cdot \left(\frac{\tilde{\sigma}_{12}}{S} \right)^2 \right]^{\frac{1}{2}} \geq 1 & (\tilde{\sigma}_{22} < 0) \end{cases} \quad (4.5)$$

where the shear contribution factor α ranges from 0 to 1.

4.4 Types of damage evolution

Once the damage is initiated in a material point of composite material, the stiffness must be degraded. This results in strain-softening of the composite materials rather than strain hardening, which is observed in metals. Several post-damage models have been proposed for progressive failure analysis, and most of them belong to one of the following categories: instantaneous unloading, gradual loading, or constant stress at failure material point, as shown in Fig.(4.2)

Since continuum damage mechanics is a methodology to predict the progressive failure behaviour of composites, non-linear gradual unloading of the composite material is adopted and simulated in this work. Therefore non-linear material properties degradation model is implemented in this work. Based on the type of damage variable chosen, i.e., scalar, vector or second-order tensor, the damage modelling can be classified into isotropic or anisotropic damage modelling. A brief description of the types of damage modelling, damage evolution equation used and material tangent stiffness etc. is given below

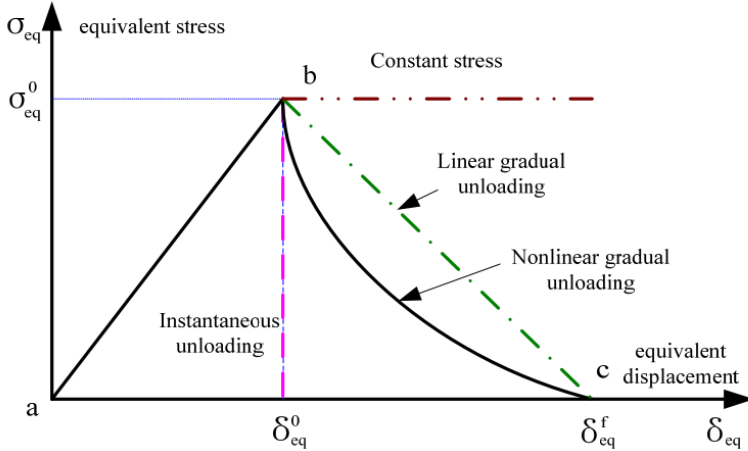


Figure 4.2: Types of degradation behaviour in damaged composite materials

4.4.1 Isotropic damage

In the case of isotropic distribution of cracks, the damage state is usually considered isotropic, and only a scalar variable D is required to represent the damage state of the material. In this work, a damage evolution law of the following form is considered for calculating damage, once the damage has been initiated

$$D = 1 - e^{-P(\tilde{\epsilon} - k)} \quad (4.6)$$

where P is the softening parameter which determines the slope of the damage evolution, $\tilde{\epsilon}$ is the 1D equivalent strain and k is the threshold value. Since the eqn. (4.6) is an exponential equation, the damage D evolves exponentially from 0 to 1, and the strain-softening will be an exponential decay function. Once the damage starts to evolve, the material property must be degraded. Therefore the material stiffness matrix of the damaged material is given by,

$$\mathbb{C}(D) = (1 - D)\mathbb{C}_0 \quad (4.7)$$

where \mathbb{C}_0 is the material stiffness matrix of the undamaged material. Therefore the stress-strain relation for a strain softening model is given by,

$$\sigma = \mathbb{C}(D) : \epsilon \quad (4.8)$$

The finite element equations obtained for the strain-softening model are non-linear. Therefore Newton-Raphson technique is used to solve the resulting system of non-linear equations. To ensure the robustness of the Newton-Raphson method, it is

important to compute the material tangent constitutive tensor \mathbb{C}_T . It can be derived as follows,

$$\begin{aligned}\mathbb{C}_T &= \frac{\partial\sigma}{\partial\epsilon} \\ \sigma &= f(\epsilon, D) \\ \mathbb{C}_T &= \mathbb{C}(D) + \epsilon : \left(\frac{\partial\sigma}{\partial D} \otimes \frac{\partial D}{\partial\epsilon} \right)\end{aligned}\quad (4.9)$$

In the above equation, the first term $\mathbb{C}(D)$ is the damaged elasticity matrix and second term is due increased damage. In the absence of damage propagation in an increment (For eg., during unloading), the material tangent tensor is equal to the damaged elasticity matrix, so the response is linearly elastic.

4.4.2 Anisotropic damage

In the case of orthotropic materials, the material property differs in the mutually perpendicular directions. Therefore it is more appropriate to choose a second-order damage tensor. In this work, a symmetric second-order tensor \underline{D} is chosen, whose principal directions are assumed to coincide with the principal material directions. The eigenvalues of the damage tensor \underline{D} have a simple physical interpretation, i.e., the i^{th} eigenvalue d_i represents the effective fractional reduction in load carrying area on planes that are perpendicular to i^{th} principal material direction. The damage tensor \underline{D} can be represented as,

$$\underline{D} = \begin{bmatrix} d_1 & 0 & 0 \\ 0 & d_2 & 0 \\ 0 & 0 & d_3 \end{bmatrix}$$

A simple exponential damage evolution law for each principal material direction in case of anisotropic damage is given as follows,

$$d_i = 1 - \frac{e^{-P(F_I-1)}}{F_I} \quad (4.10)$$

where d_i ($i = 1,2,3$) and F_I ($I = f,m,z$) are damage evolution and failure index in each principal material direction respectively. The material tangent stiffness tensor for anisotropic damage can also be derived in the same way as isotropic damage and it is given as follows

$$\mathbb{C}_T = \frac{\partial\sigma}{\partial\epsilon}$$

$$\begin{aligned}\sigma &= f(\epsilon, D) \\ \mathbb{C}_T &= \mathbb{C}(D) + \epsilon : \sum_{i=1}^3 \left(\frac{\partial \sigma}{\partial d_i} \otimes \frac{\partial d_i}{\partial \epsilon} \right)\end{aligned}\quad (4.11)$$

In the above equation, the first term $\mathbb{C}(D)$ is the degraded stiffness matrix and their matrix representation for 2D/Plane-stress and 3D are given in the section () and (). In the above equation, the second term (i.e., due to increased damage) must be computed only if the corresponding failure mode is active. Since the damage evolution equation d_i depends on the failure index, the term $\frac{\partial d_i}{\partial \epsilon}$ must be computed based on whether the corresponding damage happened during tension or compression.

4.5 Localisation and Mesh Regularisation

Finite element simulations which use continuum damage models are susceptible to mesh dependency. When the finite element discretization is refined, the numerical problems do not converge to a physically meaningful solution. Because of the strain-softening behaviour of the material, the strain tends to localize, resulting in a strong mesh dependency, i.e., the solution is non-objective with respect to mesh refinement, and the energy dissipated decreases with the decrease in finite element size. Merely improving the numerical solution schemes cannot alleviate the problem associated with mesh dependency and localization. Even if the convergence to the actual solution is improved, the solution may not even make sense from a physical point of view. Therefore the so-called fracture energy regularization is used to reduce the mesh sensitivity. In this technique, the softening law (damage evolution law) is modified so that the amount of energy dissipated over a fully degraded finite element depends on the fracture energy of the material and the finite element size. Therefore the fracture energy (G_f) of the material and characteristic length (L_c) of the finite element must be included in the damage evolution equations. The damage evolution equations based on fracture energy regularization technique for each principal direction is shown below,

In longitudinal direction 1,

$$d_1 = 1 - \frac{e^{P_1(F_f-1)}}{F_f} \quad (4.12)$$

In transverse direction 2,

$$d_2 = 1 - \frac{e^{P_2(F_m-1)}}{F_m} \quad (4.13)$$

In transverse direction 3,

$$d_3 = 1 - \frac{e^{P_3(F_z-1)}}{F_z} \quad (4.14)$$

where $P_1 = \frac{-\sigma_{11}^f \epsilon_{11}^f L_c}{G_{f,1}}$, $P_2 = \frac{-\sigma_{22}^f \epsilon_{22}^f L_c}{G_{f,2}}$ and $P_3 = \frac{-\sigma_{33}^f \epsilon_{33}^f L_c}{G_{f,3}}$

- $G_{f,i}$ - is the fracture energy in each principal direction ($i = 1,2,3$)
- σ_{ii}^f - failure strength in each principal direction ($i = 1,2,3$)
- ϵ_{ii}^f - failure strain in each principal direction ($i = 1,2,3$)
- L_c - Characteristic length

4.6 Numerical implementation of the damage model in ANSYS

As discussed before, the material models necessary for simulating progressive damage failure are implemented using the ANSYS user-programmable feature called USERMAT. The damage model implemented using USERMAT computes and updates the current stress and consistent tangent stiffness. The following sections deal with the numerical implementation of the damage model based on two different methods or criteria used to predict the damage initiation.

- Strain based damage model
- Stress based damage model

4.6.1 Strain based damage model

In the case of the strain-based damage model, the damage initiation is predicted using current strain (ϵ_{n+1}). The USERMAT receives strains, stresses and state variables at the beginning of the time increment and the current strain increment. The following steps describe the process of implementing the damage model

- Calculate current strain

$$\underline{\epsilon}_{n+1} = \underline{\epsilon}_n + \Delta \underline{\epsilon}$$

- Calculate the current degraded material stiffness matrix $\mathbb{C}(\underline{D}_n)$
- Calculate the failure indices $F_I(\underline{\epsilon})$ (Refer to Sections (??) and (4.3.1))

Check if $F_I \geq F_{I\max}$

- if $F_I(\underline{\epsilon}) < 1$

$$\underline{\sigma}_{n+1} = \mathbb{C}(\underline{D}_n) : \underline{\epsilon}_{n+1}$$

$$\mathbb{C}_T = \mathbb{C}(\underline{D}_n)$$

- else

Calculate the damage variables using damage evolution law, (Refer to eqn (4.12) to (4.14))

$$d_1(F_f), d_2(F_m), d_3(F_z)$$

Check if $d_i \geq 0$

Calculate the updated degraded stiffness based on damage variables

$$\mathbb{C}(\underline{D}_{n+1})$$

Calculate current stress

$$\underline{\sigma}_{n+1} = \mathbb{C}(\underline{D}_{n+1}) : \underline{\epsilon}_{n+1}$$

Calculate tangent stiffness

$$\mathbb{C}_T = \mathbb{C}(D) + \sum_{i=1}^3 \left(\frac{\partial \mathbb{C}(D)}{\partial d_i} : \epsilon \otimes \frac{\partial d_i}{\partial \epsilon} \right)$$

4.6.2 Stress based damage model

In the case of stress-based damage model, the damage initiation is predicted using effective stress ($\tilde{\sigma}_{n+1}$). The USERMAT receives strains, stresses and state variables at the beginning of the time increment and the current strain increment. The following steps describe the process of implementing the damage model.

- Calculate the elastic stiffness matrix \mathbb{C}
- Calculate effective stress

$$\tilde{\sigma}_{n+1} = \mathbb{C}_0 : \underline{\epsilon}_{n+1}$$

- Calculate the failure indices $F_I(\underline{\sigma})$, (Refer to Section (4.3.2) and (4.3.3))

Check if $F_I \geq F_{I\max}$

- if $F_I(\underline{\sigma}) < 1$

$$\underline{\sigma}_{n+1} = \tilde{\sigma}_{n+1}$$

$$\mathbb{C}_T = \mathbb{C}$$

- else

Calculate the damage variables using damage evolution law, (Refer eqn (4.12) to (4.14))

$$d_1(F_f), d_2(F_m), d_3(F_z)$$

Check if $d_i \geq 0$

Calculate the updated degraded stiffness based on damage variables

$$\mathbb{C}(\underline{D}_{n+1})$$

Calculate current stress

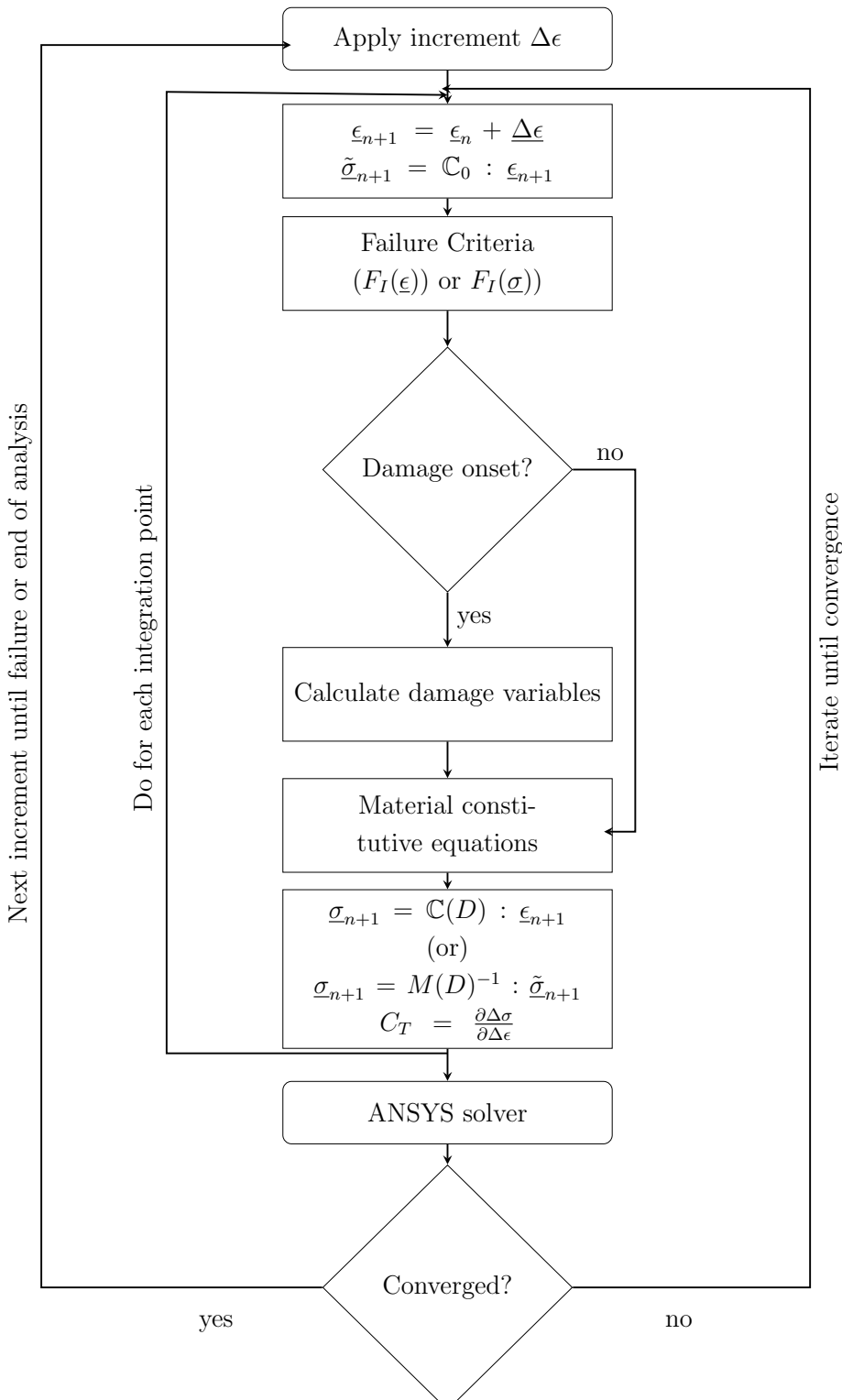
$$\underline{\sigma}_{n+1} = M(D)^{-1} : \tilde{\underline{\sigma}}_{n+1}$$

Calculate tangent stiffness

$$\mathbb{C}_T = \mathbb{C}(D) + \sum_{i=1}^3 \left(\frac{\partial \mathbb{C}(D)}{\partial d_i} : \epsilon \otimes \frac{\partial d_i}{\partial \epsilon} \right)$$

4.7 Schematic of UMAT implementation

The flowchart below shows the schematic of the user material subroutine (USERMAT) implementation for both and strain and stress based damage model and how the subroutine interacts with the ANSYS environment.



Chapter 5

Results and Discussion

5.1 Modelling linear elastic behaviour of orthotropic materials

Before implementing the damage behaviour in orthotropic materials, their linear elastic behaviour must be implemented which describes what happens before the damage initiation. As mentioned before orthotropic materials are a special class of material whose properties differ in mutually perpendicular directions. Therefore 9 independent material constants are required to model their elastic behaviour. Table (5.1) summarises the utilised material parameters. The material parameters presented here belong to an unidirectional glass fiber-reinforced epoxy material. In this material, the strength in the longitudinal direction (X_t and X_c) is very high compared to the transverse directions (Y_t and Y_c) because the fibers are aligned parallel to the longitudinal direction. The constitutive matrix given in the section (2.9) and Hooke's law help us model the elastic behaviour of the orthotropic materials.

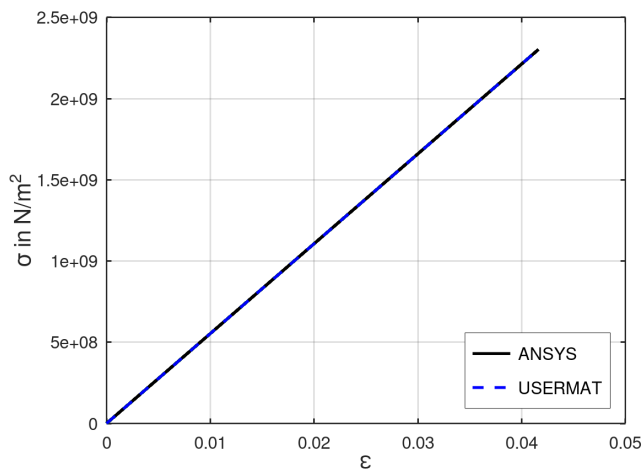
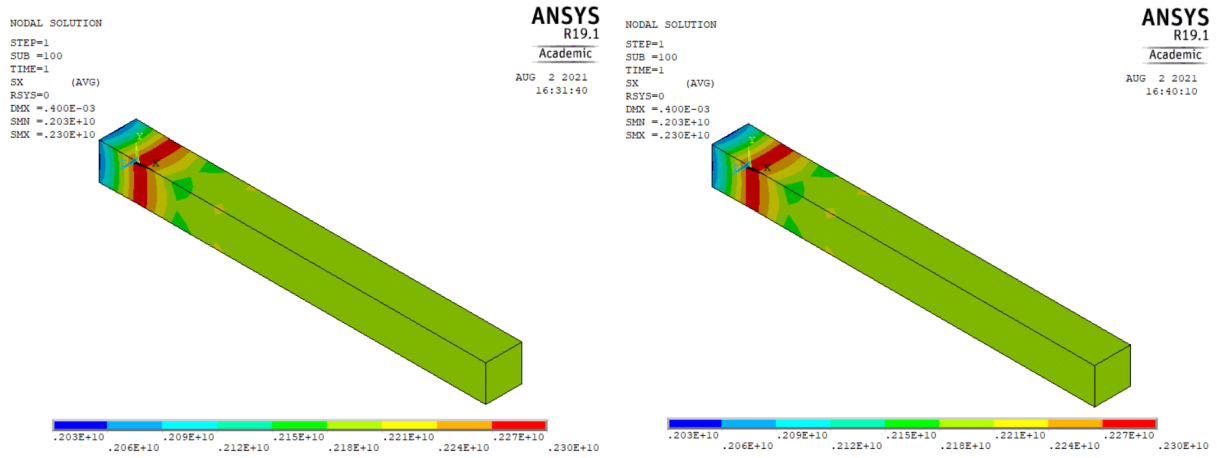


Figure 5.1: Stress-Strain relation (Standard vs user-defined material routine)

Symbol	Material Parameter	Value
E_1	Elastic modulus in longitudinal (1) direction	55000e6 N/m ²
$E_2 = E_3$	Elastic modulus in transverse (2 and 3) directions	9500e6 N/m ²
$\nu_{12} = \nu_{13}$	Poisson's ratio (in-plane)	0.33
ν_{23}	Poisson's ratio (Planes 2-3)	0.27
$G_{12} = G_{13}$	In-plane shear modulus	5500e6 N/m ²
G_{23}	Shear modulus (Planes 2-3)	3000e6 N/m ²
X_t	Tensile strength in longitudinal (1) direction	2500e6 N/m ²
X_c	Compressive strength in longitudinal (1) direction	-2000e6 N/m ²
Y_t	Tensile strength in transverse (2 and 3) directions	50e6 N/m ²
Y_c	Compressive strength in transverse (2 and 3) directions	-200e6 N/m ²
S_{12}	In-plane strength	50e6 N/m ²

Table 5.1: Material parameters (Integration point studies)

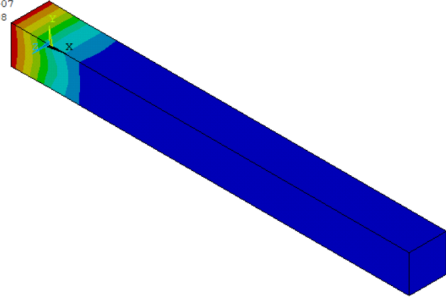
The linear elastic behaviour of the orthotropic material is implemented in the USERMAT using constitutive equations, and in this section, the results obtained are compared against the standard orthotropic material option present in ANSYS using a structural example. A bar of length 10 mm and area 1 mm² ($b = 1$ mm, $t = 1$ mm) fixed at one end is chosen for the analysis. The bar is constructed using 8 node SOLID 185 elements, and full integration has been used. A displacement of 1 mm is applied at the free end, and the results obtained using the standard and the user-defined material routines are presented below. Figure (5.1) compares the stress-strain relation of the bar obtained using both ANSYS default and USERMAT



```

NODAL SOLUTION
STEP=1
SUB =100
TIME=1
SY (AVG)
RSYS=0
DMX = .400E-03
SMN =-.732E+07
SMX =.778E+08

```

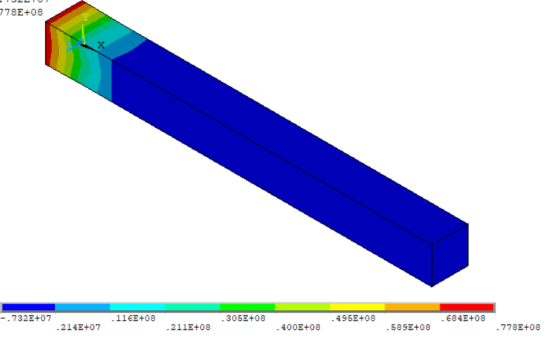


(c) Y Component of Stress

```

ANSYS
R19.1 NODAL SOLUTION
Academic
STEP=1
SUB =100
TIME=1
SY (AVG)
RSYS=0
DMX = .400E-03
SMN =-.732E+07
SMX =.778E+08

```

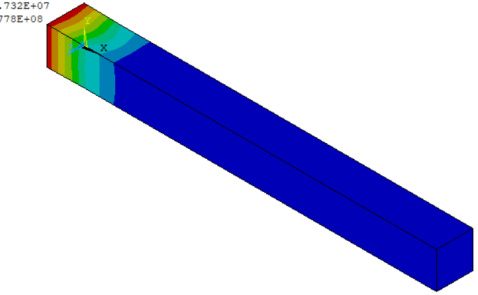


(d) Y Component of Stress

```

NODAL SOLUTION
STEP=1
SUB =100
TIME=1
SZ (AVG)
RSYS=0
DMX = .400E-03
SMN =-.732E+07
SMX =.778E+08

```

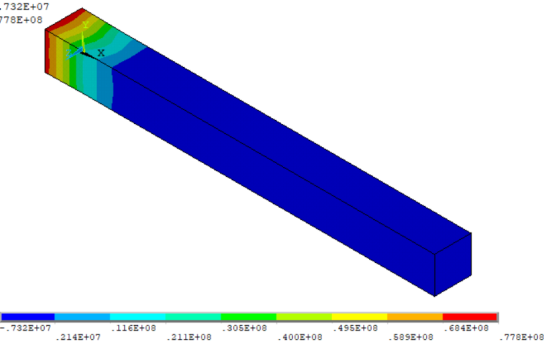


(e) Z Component of Stress

```

ANSYS
R19.1 NODAL SOLUTION
Academic
STEP=1
SUB =100
TIME=1
SZ (AVG)
RSYS=0
DMX = .400E-03
SMN =-.732E+07
SMX =.778E+08

```



(f) Z Component of Stress

Figure 5.2: Contour plots of the stress components σ_{11}, σ_{22} and σ_{33} of the bar obtained using standard (Figures a,c,e on the left) and user-defined material routine (Figures b, d, f on the right)

Figure (5.2) shows the contour plots of the normal stresses (σ_{11} , σ_{22} and σ_{33}) computed using standard and user-defined material routine respectively. The comparison of the stress-strain relation and contour plots between the standard and user-defined material routine confirms that the results obtained using both options are same and therefore further damage-initiation and damage-evolution processes can now be implemented.

5.2 Damage behaviour at integration point level

The material subroutines are first developed on the OCTAVE and tested using constitutive driver routines, enabling us to understand the phenomenon at the integration point level. To demonstrate the evolution of damage after damage

initiation and the strain-softening, following simple loading cases are investigated at the integration point level.

- Uniaxial tension
- Biaxial tension
- Triaxial tension.

After that, the material subroutines are implemented in USERMAT and tested in the ANSYS environment using a 3D finite element of unit length. The finite element is subjected to the above loading cases, and the results are compared against the OCTAVE implementation

5.2.1 Uniaxial tension

In the case of uniaxial tension, the normal stress is present only in one direction, and two other normal stresses and all the shear stresses are zero, i.e., only one non-zero component is located on the main diagonal of the stress tensor is . In the ANSYS environment, uniaxial tension is achieved by applying a displacement on the finite element in a normal direction (1), which increases the strain ϵ_{11} linearly, and the lateral (transverse) contraction is not constrained. 3D Hashin's quadratic strain criteria (Section(4.3.1)) are used to predict the damage initiation, and the exponential damage evolution law (Eqn(4.10)) is used to calculate the damage evolution. The results obtained from ANSYS and USERMAT are presented in Figure (5.3a) and (5.3b) respectively. Figure (5.4) shows the evolution of damage variables.

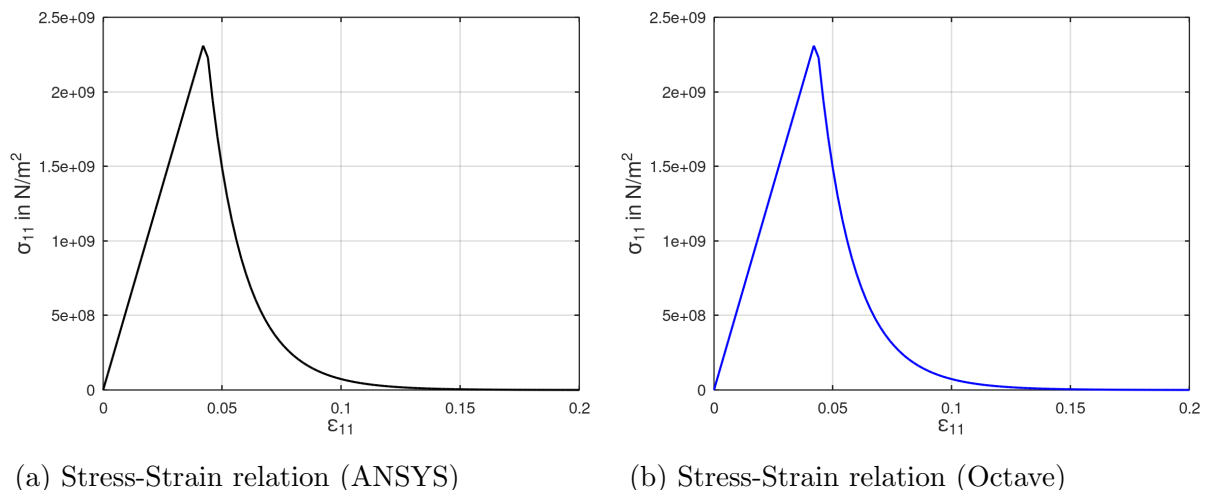


Figure 5.3: Evolution of stress for uniaxial tension test in 11 direction

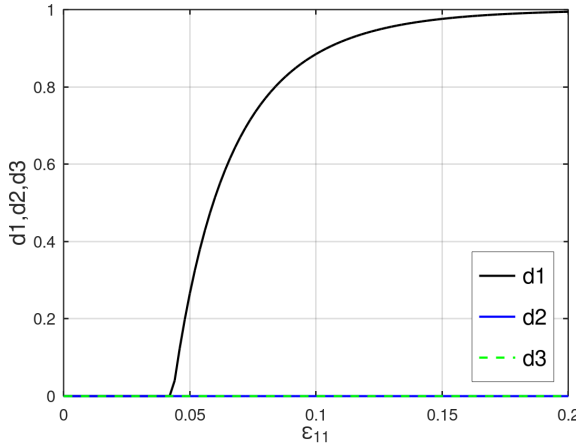


Figure 5.4: Evolution of damage components for uniaxial tension test in 11 direction

The system is linearly elastic until the damage initiation strain, and the damage is zero. Once the strain ϵ_{11} exceeds the damage initiation strain, the damage d_1 starts to evolve exponentially, and the stress starts to drop due to the reduction in stiffness in 1 direction. The damage variables d_2 and d_3 are zero. The comparison between the figures (5.3a) and (5.3b) suggests that the material routine implemented in OCTAVE and USERMAT are numerically similar to each other. The scalar softening parameter (P) in the damage evolution equation(4.10) determines the slope of the damage curve. The following figure demonstrates the influence of the softening parameter (P) on the damage evolution

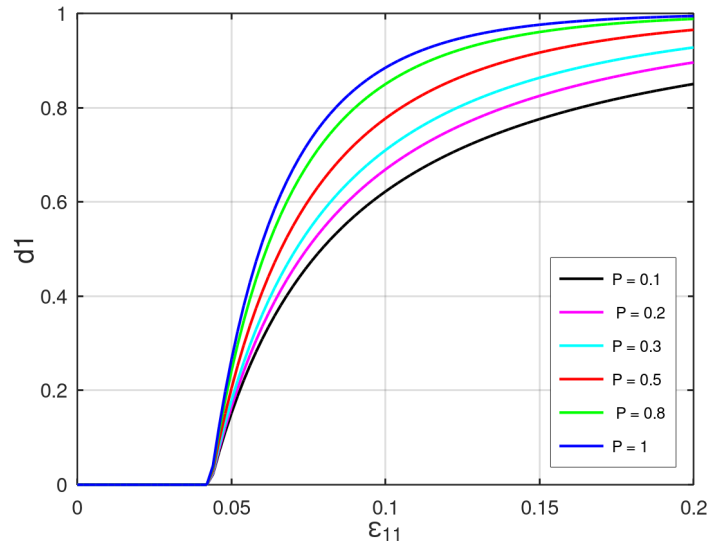


Figure 5.5: Influence of softening parameter P in the damage evolution)

Drawbacks of strain based damage initiation criteria

Since the lateral contraction is not constrained during uniaxial tension, the transverse directions experience negative strain due to Poisson's effect, i.e., ϵ_{22} and ϵ_{33} will be negative. If the compressive strength in the transverse directions 2 and 3 are sufficiently low, the strains ϵ_{22} and ϵ_{33} will exceed the damage initiation strain. This leads to damage evolution without the presence of stress in transverse directions 2 and 3. This phenomenon cause convergence issues and the computation stops when the damage evolves without the presence of stress. Figure (5.6) shows the norm of the residual stress, which does not reach zero (or a tolerance) after 100 iterations of the Newton-raphson, which indicates the failure of the model to converge to a solution when using low compressive strength in the transverse direction ($Y_c = -180\text{MPa}$)

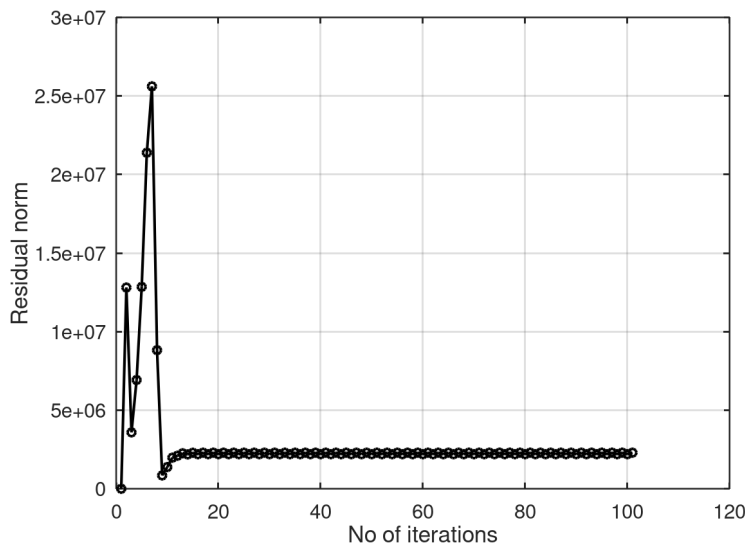


Figure 5.6: Convergence issue: Residual norm of the stress *vs* No of Newton-raphson iterations

This problem can be rectified by using stress-based damage initiation criteria. Since damage evolution depends on failure index F , the transverse failure indices F_m and F_z will be zero during uniaxial tension if the stress-based damage initiation criteria are used. This results in zero damage in the transverse direction. The following section presents the results obtained using stress-based damage initiation and the use of mesh regularisation in the damage evolution law.

Stress based damage initiation and mesh regularisation

As mentioned in section (4.5), the strain localisation problems result in strong mesh dependency, so fracture energy and characteristic length (L_c) of the element

have to be included in the damage evolution law in order to alleviate the problem. So the material routine is modified by changing the damage initiation criteria to maximum stress criteria (4.1) and including the damage evolution equations from (4.12) to (4.14). The uniaxial tension is conducted again with the changes mentioned above and with very low transverse compression strength, and the results are presented below.

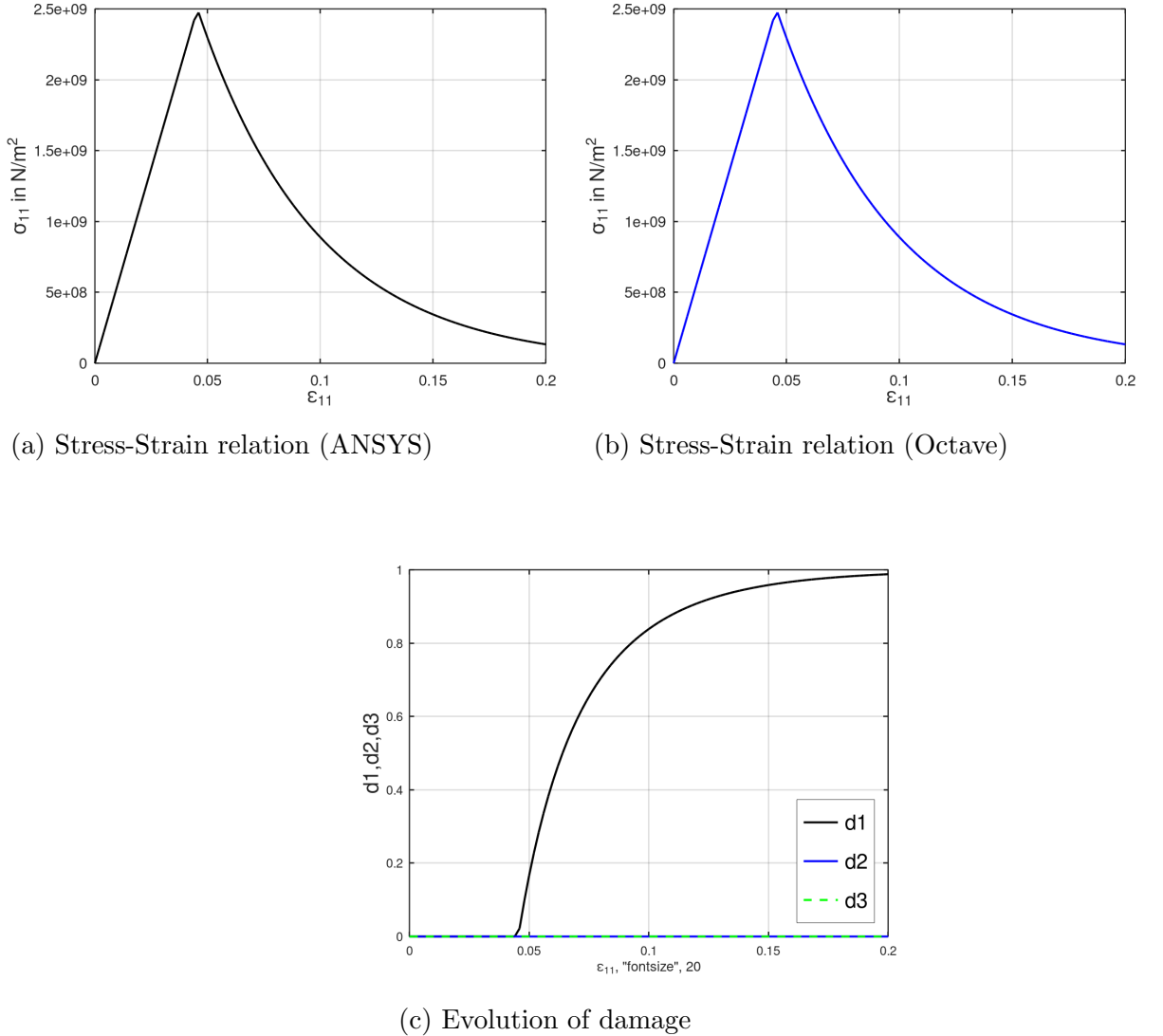


Figure 5.7: Evolution of stress and damage components with stress-based damage initiation criteria under uniaxial tension

From figure (5.7c) it is evident that the damage d_2 and d_3 are zero as a result of stress-based damage initiation because the stress components σ_{22} and σ_{33} are zero under uniaxial tension. While using mesh regularisation, the slope of the damage curve is determined by the characteristic length (L_c), which depends on the volume of the element. The following figure (5.5) shows how the damage evolution is affected by the volume of the element,

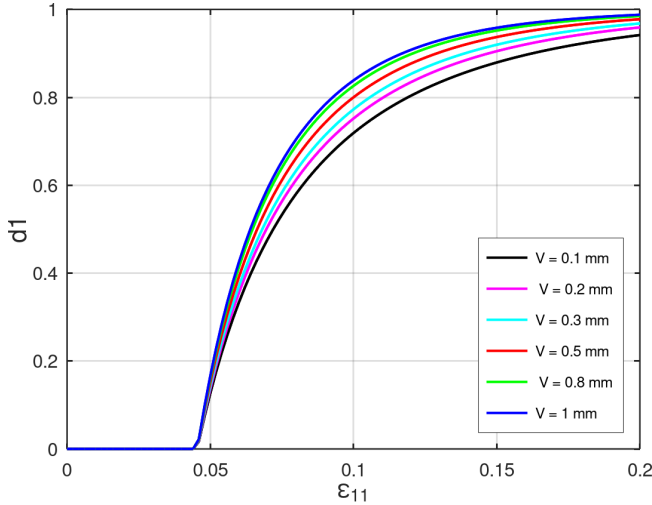


Figure 5.8: Influence of element volume (V) on the damage evolution

Discussion of tangent stiffness

In the case of uniaxial tension, the components of the stress tensor other than σ_{11} are zero. Since stress conditions are enforced, the OCTAVE driver routine uses the Newton-raphson method to determine the input strain components other than ϵ_{11} iteratively. The Newton-raphson method requires a tangent stiffness for computation which can be derived using the equation (4.11) for anisotropic damage. This enables us to test the derived algorithmic tangent stiffness (ATS) before implementing it in USERMAT. The derived algorithmic tangent stiffness is verified by comparing it with the numerical tangent stiffness computed using numerical perturbation. In numerical perturbation, the coefficients of the strain tensor are perturbed by a very small value, i.e., $\Delta\epsilon_{kl}^{n+1} = \delta$ (where $\delta \ll 1$) and the resulting stress perturbations are calculated.

$$\Delta\sigma_{ij}^{n+1} = \sigma_{ij}^{n+1}(\epsilon_{kl}^{n+1} + \delta) - \sigma_{ij}^{n+1}(\epsilon_{kl}^{n+1}) \quad (5.1)$$

Then the components of the tangent stiffness tensor can be estimated as

$$C_T = \frac{\Delta\sigma_{ij}^{n+1}}{\Delta\epsilon_{kl}^{n+1}} \quad (5.2)$$

Since the material routine must be evaluated for every perturbation of ϵ_{kl} the routine has to be called six time recursively per load-step iteration. The figure (5.9a) and (5.9b) shows the strain components ϵ_{22} and ϵ_{33} computed using algorithmic and numerical tangent stiffness which are plotted against ϵ_{11} respectively.

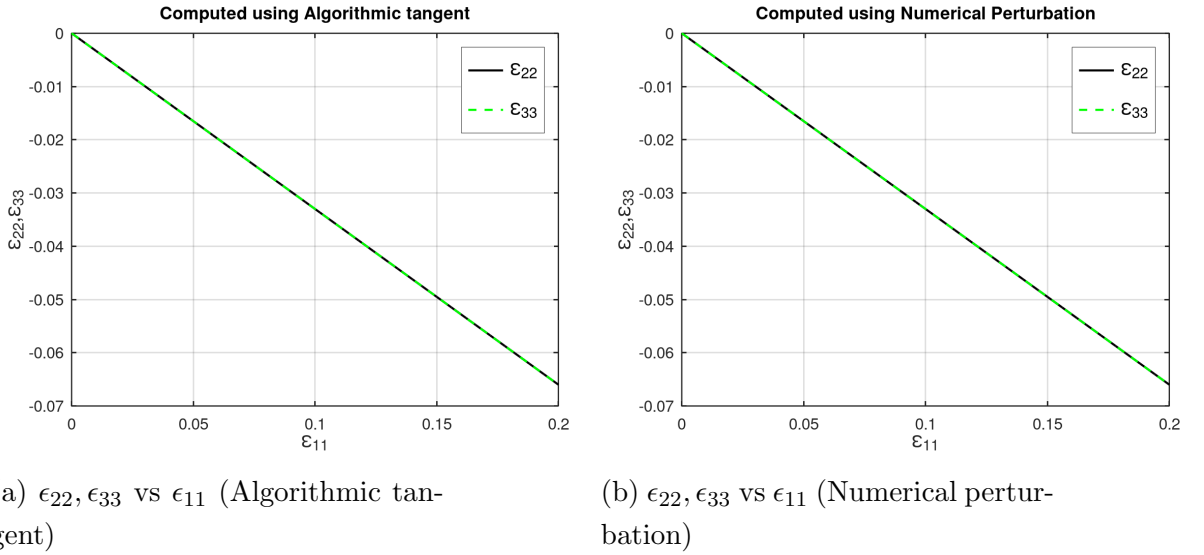
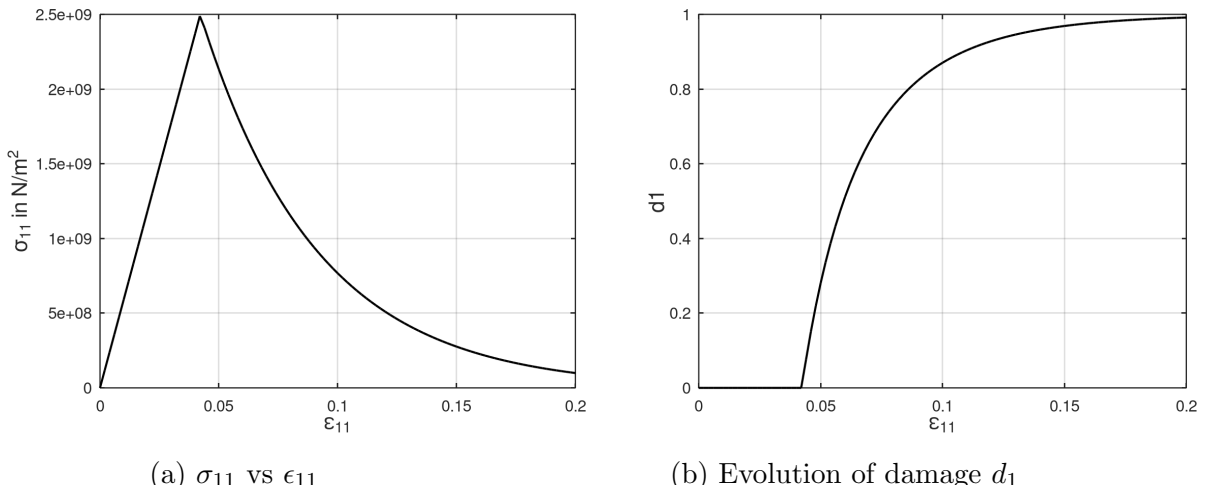


Figure 5.9: The strain components ϵ_{22} and ϵ_{33} computed using algorithmic (a) and numerical tangent stiffness (b) under uniaxial tension

These comparison between above plots clearly indicates that the tangent stiffness computed using algorithmic tangent and numerical tangent are numerically similar to each other.

5.2.2 Biaxial tension

In the case of biaxial tension, normal stresses are present only in two normal directions, and all the shear stresses are zero as well as the normal stress in third direction, i.e., only two non-zero components presented located on the main diagonal of the stress tensor . In ANSYS, biaxial tension is achieved by applying the same displacements in two normal directions of the finite element (1 and 2 direction), and the contraction in the third direction (3) is unconstrained. The following figures show the corresponding stress and damage components obtained from the test.



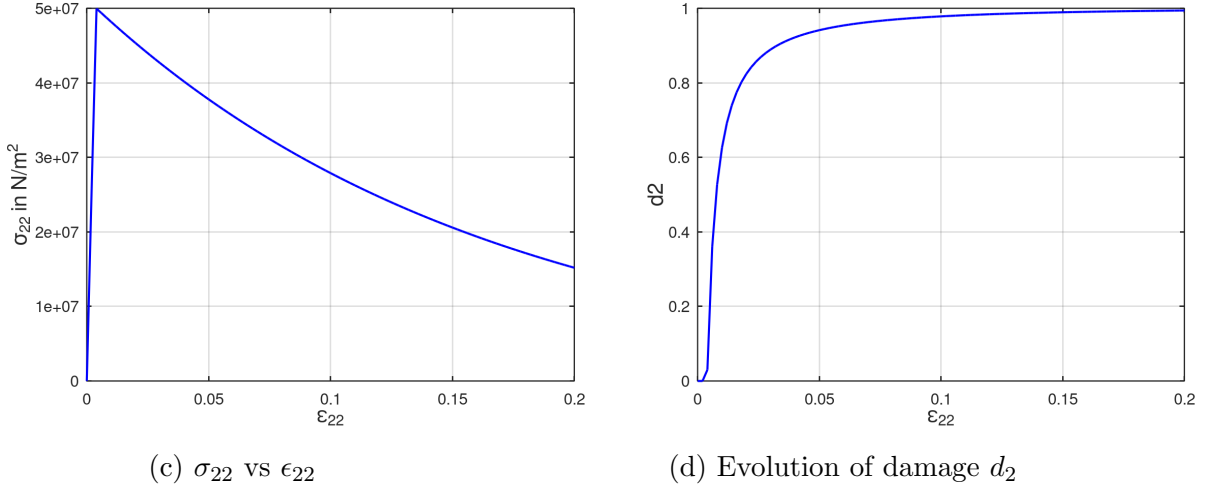
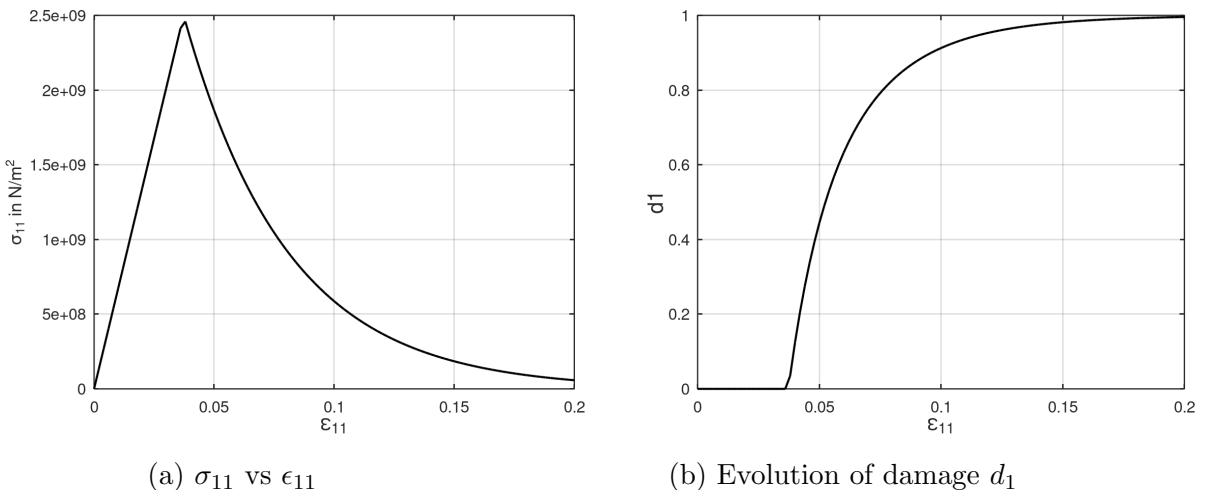


Figure 5.10: Evolution of stress (Figures a, c on the left) and corresponding damage (Figure b, d on the right) components under biaxial tension

Since the tensile strength in transverse direction is very low compared to the longitudinal direction, evolution of damage (d_2) begins very soon and simultaneously the stress component (σ_{22}) drops as seen in figures (5.10c) and (5.10d).

5.2.3 Triaxial tension

In the case of triaxial tension, the normal stresses are present in all three normal directions, and all the shear stresses are zero, i.e., only diagonal components of the stress tensor are non-zero. In Ansys, triaxial tension is achieved by applying the same displacement in all three normal directions (1, 2 and 3 direction). The following figures show the corresponding stress and damage components obtained from the test.



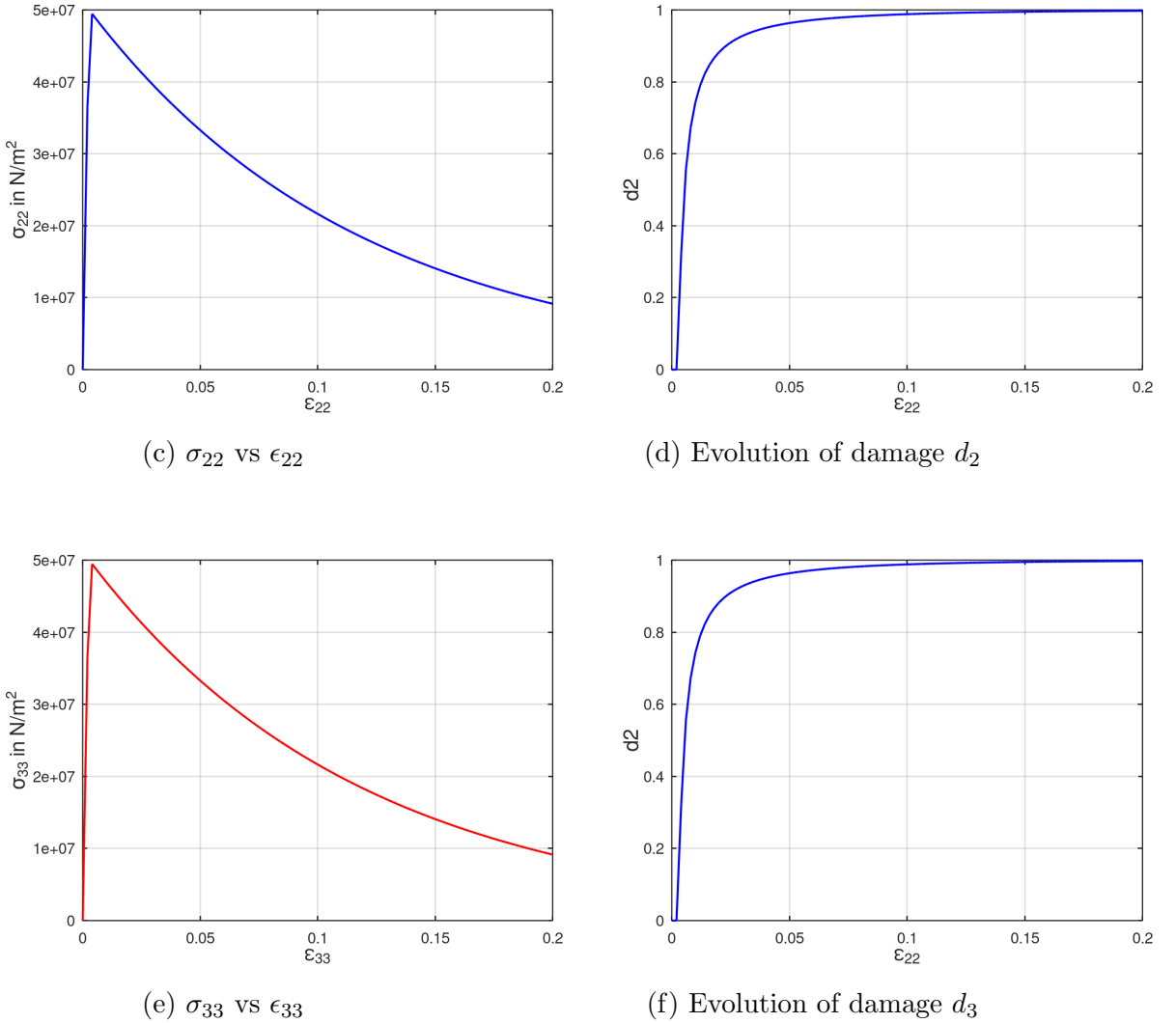


Figure 5.11: Evolution of stress (Figures a, c, e on the left) and corresponding (Figures b ,d, f on the right) damage components under triaxial tension

Since the material properties are the same in transverse 2 and 3 direction and the tensile strength is very low compared to the longitudinal 1 direction, the damage d_2 and d_3 evolves simultaneously (Figure (5.11d) and (5.11f)) and very soon as expected. Therefore the stress components σ_{22} and σ_{33} drop very soon as shown in Figure (5.11c) and (5.11e)

5.3 Representative structural examples

The following structural examples are used to test the damage model implemented as a USERMAT in the ANSYS environment

- Notched tensile specimen (2D - Plane stress)
- Compact tension (CT) specimen (2D - Plane stress)

- Plate with hole (3D)

Each example is chosen to demonstrate specific features of the damage model. These features include, at first, the capability of the model to represent damage initiation and propagation and secondly, the calculation of multiple damage variables, i.e., the ability to show anisotropic damage development in the composite material when a load is applied, both in 2D and 3D setting. Furthermore, mesh convergence studies are performed to show that the regularization scheme employed gives better results than the model with no regularization. For all the finite element simulations of the above models, linear quadrilateral elements are used (both 2D and 3D) with full Gauss integration. The line search option has been enabled during all the simulations to get good convergence behaviour. The material used for the finite element simulations is T700/2510 carbon fiber/epoxy fabric. The material has fibers in parallel in the longitudinal direction and fibers woven in the cross-section that provide additional strength in transverse directions. The material has a high modulus and strength in the longitudinal direction because of the presence of a large number of fibers. The material properties are obtained from and a summary of the material properties are given in the Table (5.2).

Symbol	Material Parameter	Value
E_{11}	Modulus in longitudinal (1) direction	55.8 GPa
$E_{22} = E_{33}$	Modulus in transverse (2 and 3) directions	54.9 GPa
ν_{12}	Poisson's ratio	0.043
$G_{12} = G_{23} = G_{13}$	Shear modulus	4.2 GPa
X_t	Tensile strength in longitudinal (1) direction	910.1 MPa
X_c	Compressive strength in longitudinal (1) direction	-710.2 MPa
Y_t	Tensile strength in (2 and 3) directions	772.2 MPa
Y_c	Compressive strength in (2 and 3) directions	-703.3 MPa
S_{12}	In-plane strength	131 MPa
G_f^{lt}	Tensile fracture energy along longitudinal (1) direction	125 KJ/m ²
G_f^{lc}	Compressive fracture energy along longitudinal (1) direction	250 KJ/m ²
G_f^{tt}	Tensile fracture energy along (2 and 3) directions	95 KJ/m ²
G_f^{tc}	Compressive fracture energy along (2 and 3) directions	254 KJ/m ²

Table 5.2: Material parameters (Representative structural examples)

5.3.1 Notched tensile specimen

The first example demonstrates the model's capability to represent damage initiation and propagation. A notched tensile specimen is widely used for analysis of stress concentration, fatigue etc., Because of the symmetry, only one-quarter of the specimen is modelled in the finite element analysis and the geometry and boundary conditions are shown in the Figure (5.12). The meshes consist of plane-stress elements (PLANE 182) with bilinear interpolations for displacements, and 2×2 Gauss integration has been utilized. Three different finite element meshes have been used in the fracture zone with the elements of $h=1$ mm, 0.5 mm, 0.25 mm and a total of 500, 840, 1460 elements respectively for the convergence studies (Figure 5.13). At first, the longitudinal direction is kept parallel to the loading direction, and the behaviour of the model is analyzed by applying a displacement controlled load (U_x) in the longitudinal direction (X-direction). The maximum stress criterion (Section 4.3.2) has been used to predict the damage initiation.

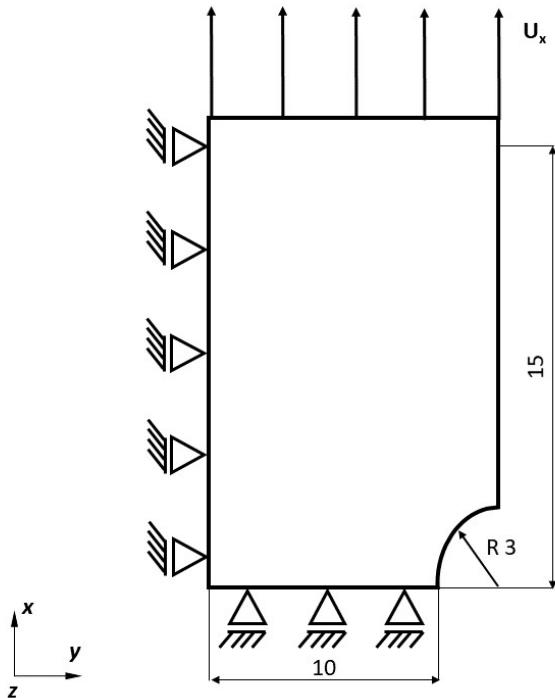


Figure 5.12: Specimen geometry and boundary conditions. Dimensions are given in mm. Displacement controlled loading U_x is applied.

The force-displacement response for the three different meshes with and without the regularization (Section(4.5)) schemes have been plotted in Figure (5.14a) and (5.14b) respectively. The global force-displacement response is characterized by a large linear regime followed by a gradual drop of the load (because of the softening) or a sudden drop in case of no regularization. From Figure (5.14), it is clearly evident that the model with regularization gives a more stable force-displacement response

compared to the model without regularization, where the maximum load capacity is very low, and the load drops significantly with the decrease in mesh size (i.e., increase in the number of elements). Even though the regularization scheme does not fully alleviate the mesh dependency, it improves the solution significantly compared to the material model without regularization.

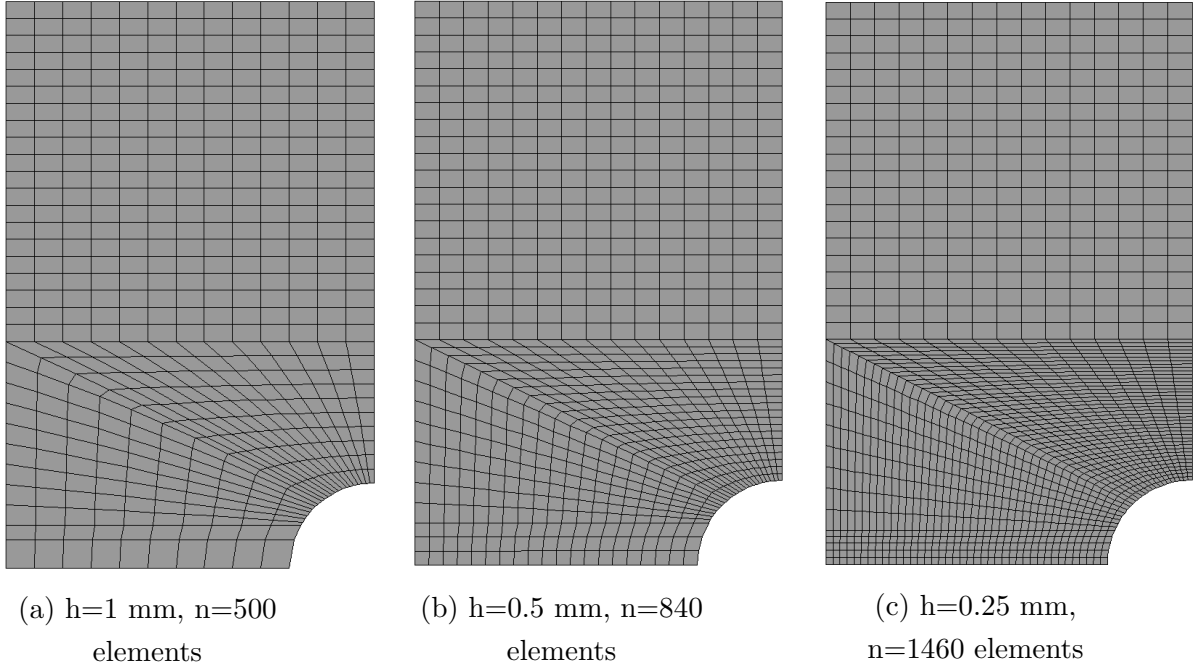


Figure 5.13: Considered meshes (h is the length of the element along fracture zone and n the total number of elements)

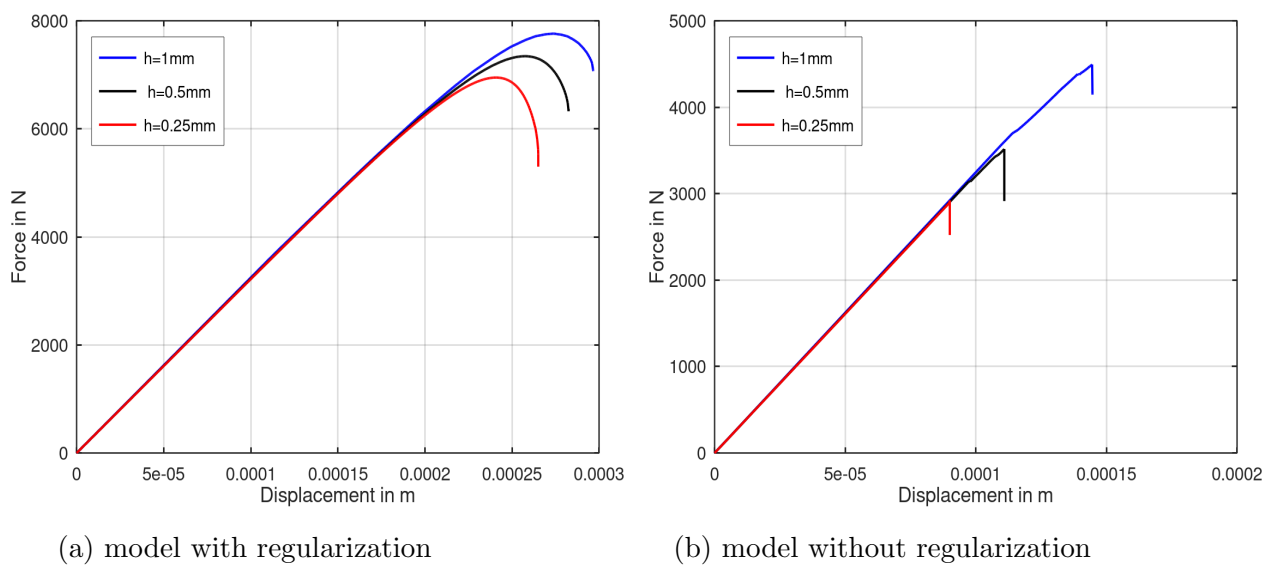
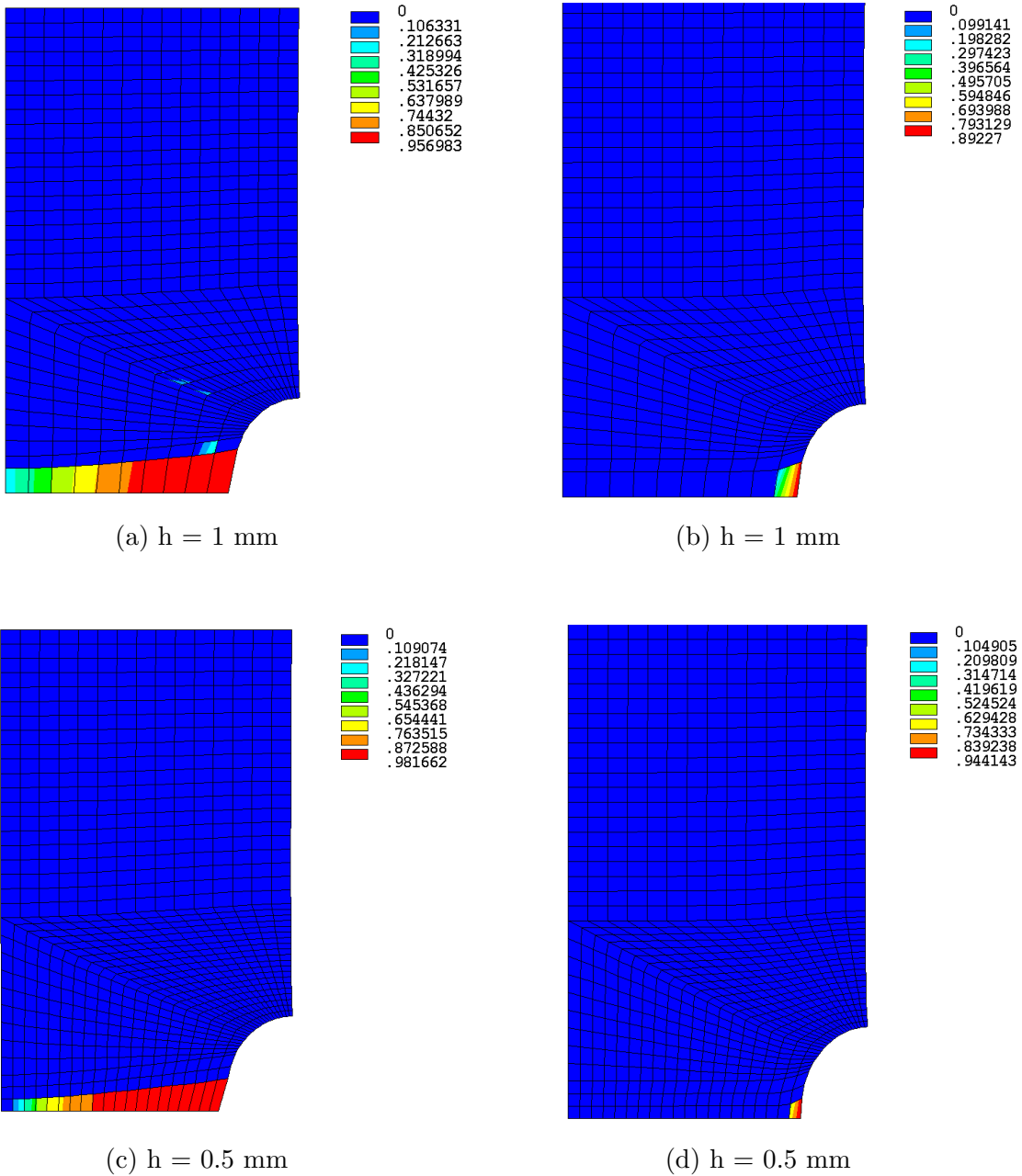
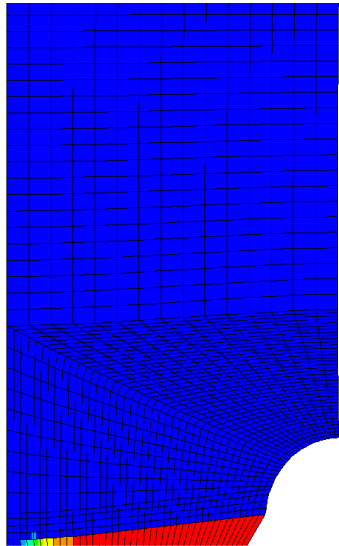


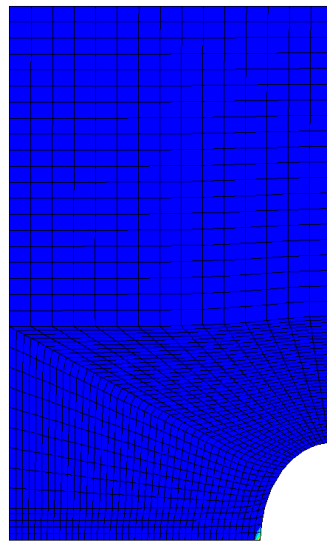
Figure 5.14: Convergence study: Global force-displacement response for model with regularization (Figure a on the left) and without regularization (Figure b the right)

The damage distributions at the end of the process have been plotted for the three different meshes in the Figure (5.15). For numerical reasons the maximum damage is limited to a threshold value of $d_{max} = 0.999$. The improvement in the global response by using regularization schemes has been illustrated by the damage distributions at the end of the loading process. A relatively large portion of the fracture zone takes part in the damage process instead of very few elements (one or two elements) in the case of no regularization. Damage initiates at the tip of the blunt notch and propagates perpendicular to the loading direction. The width of the damage zone is approximately the same in the three discretizations, but the number of elements that reach a critical damage value (red) increases with the increase in the number of elements along the fracture zone.





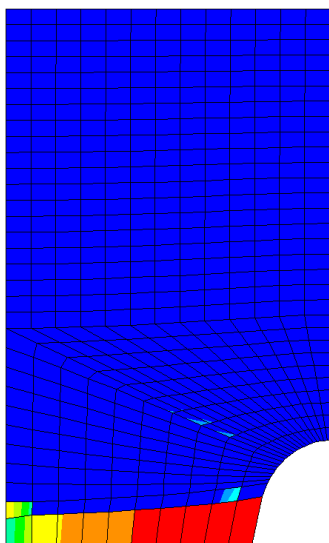
(e) $h = 0.25 \text{ mm}$



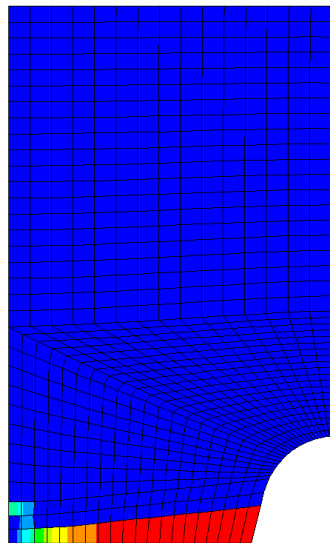
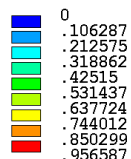
(f) $h = 0.25 \text{ mm}$

Figure 5.15: Convergence study for model with(Figure a,c,e) and without(b,d,f) regularization: Damage contour plots d_1 at the end of the loading

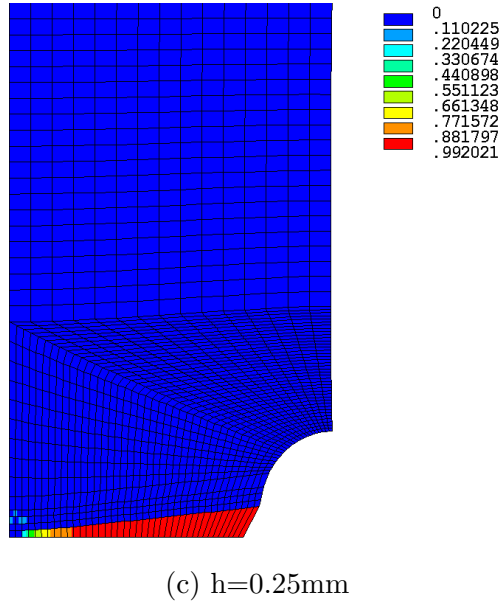
Now the transverse direction is kept parallel to the loading direction, and the behaviour of the damage model, i.e., initiation and propagation of damage d_2 , is analysed by applying a tensile load in the transverse direction. The damage (d_2) at the end of the loading process is shown in the Figure (5.16)



(a) $h=1\text{mm}$



(b) $h=0.5\text{mm}$



(c) $h=0.25\text{mm}$

Figure 5.16: Damage contour plots d_2 at the end of the loading (Loading in transverse direction)

The damage pattern looks similar to the distribution of damage (d_1) when loaded in the longitudinal direction. The force-displacement response of both longitudinal and transverse loading for a single mesh type ($h = 0.5\text{mm}$) is compared in the Figure (5.17). As expected, the maximum load capacity is high in the longitudinal direction compared to the transverse direction.

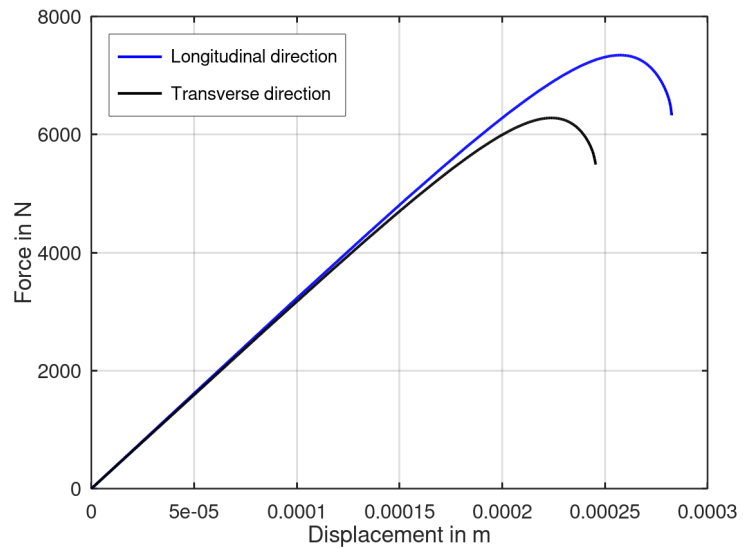


Figure 5.17: Comparison of force-displacement response in longitudinal and transverse direction for $h=0.5\text{mm}$ discretization

5.3.2 Compact Tension (CT) Specimen

This second example demonstrates the model's ability to compute multiple damage variables simultaneously, i.e., show the anisotropic damage development when a load is applied. In the plane stress (2D) setting, two damage variables (d_1 and d_2), one in each principal direction, are employed to represent the anisotropic damage development. The Compact Tension test is a standard test for plane fracture of materials and the measurement of fatigue crack growths. Because of the symmetry, only one half of the specimen is modelled, and the geometry and appropriate boundary conditions are given in Figure (5.18). The mesh consists of plane stress (PLANE 182) elements with bilinear interpolations for displacements, and 2×2 Gauss integration has been utilized. Just like the notched tensile specimen, three different finite element meshes have been used in the fracture zone with the elements of size $h = 1$ mm, 0.5 mm and 0.25 mm and a total of 509, 1409, 4811 elements, respectively for the convergence studies (Figure 5.19). A node is created at the centre of the pinhole, and the innermost nodes of the pinhole contour are connected to this node by rigid coupling option in ANSYS. A displacement controlled load (U_x) is applied at the central node, and the global force-displacement response can be obtained from this central node. At first, the longitudinal direction is kept parallel to the loading direction, and the behaviour of the model is analyzed.

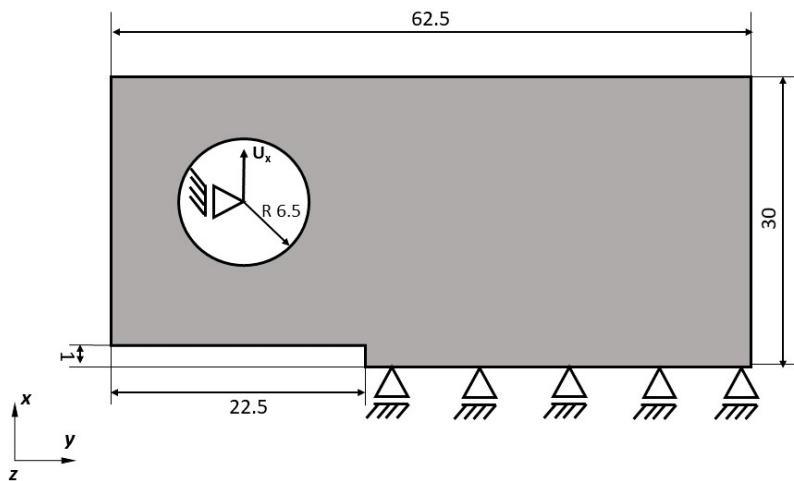
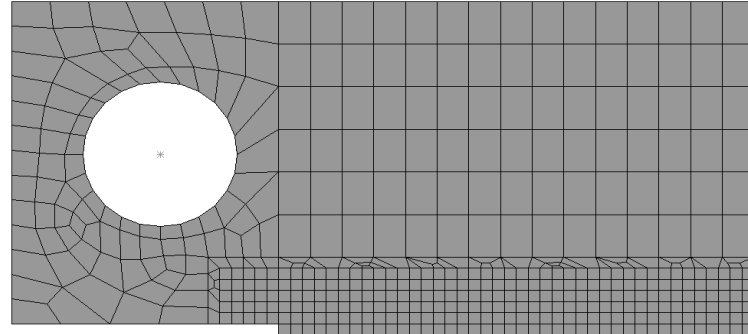


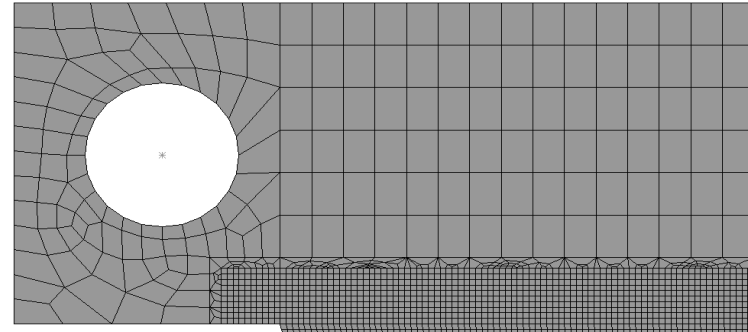
Figure 5.18: Specimen geometry and boundary conditions. Dimensions are given in mm. Displacement controlled loading U_x is applied

The global force-displacement response has been plotted for the three different meshes in Figure (5.20). As expected, the maximum load capacity decreases slightly with the decrease in mesh size (i.e., increase in the number of elements) because of the mesh sensitivity. The distributions of the damage variables d_1 and d_2 at the end of the loading process for the three different meshes have been plotted

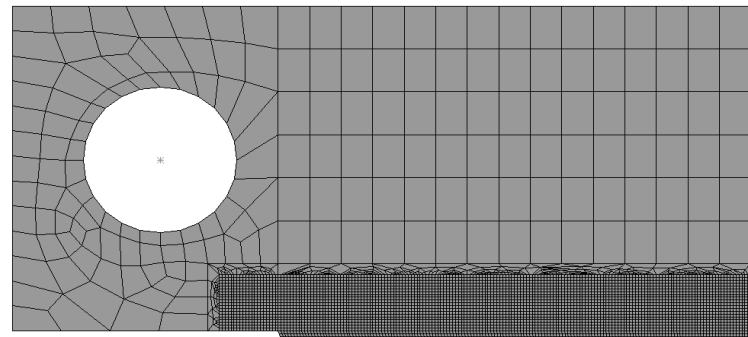
in Figure (5.21). The damage d_1 is caused by tension in the longitudinal direction and d_2 by tension in the transverse direction. The width of the damage zone for d_1 is approximately the same in all three discretizations. When the damage d_1 reaches the maximum threshold value in almost all the distorted elements, the simulations terminates; therefore, the maximum value and distribution of the damage variable d_2 depends on the size of the elements. From Figures (5.21b), (5.21d) and (5.21f) it is clearly evident that the maximum value and the width of the damage zone for d_2 increases with decrease in mesh size.



(a) $h=1 \text{ mm}$



(b) $h=0.5 \text{ mm}$



(c) $h=0.25 \text{ mm}$

Figure 5.19: Considered meshes (h is the length of the element along fracture zone and n the total number of elements)

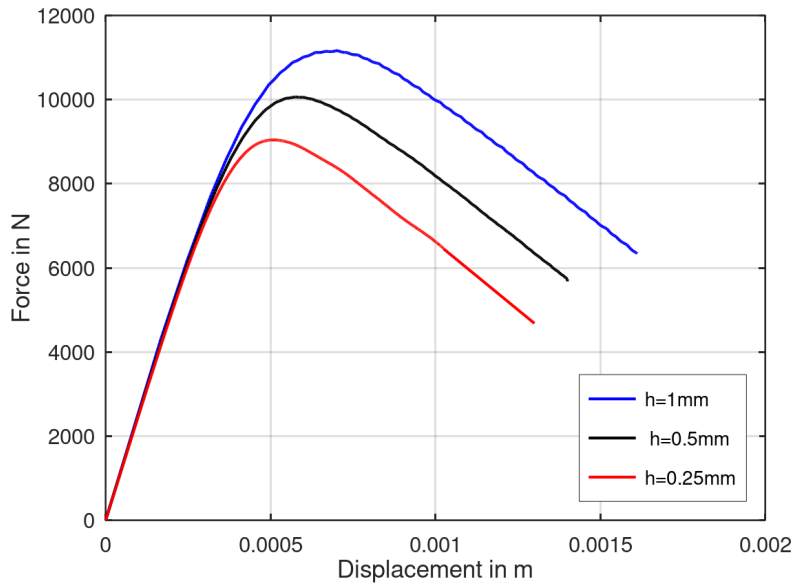
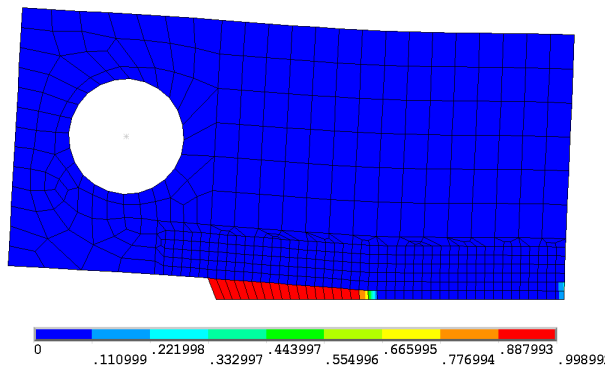
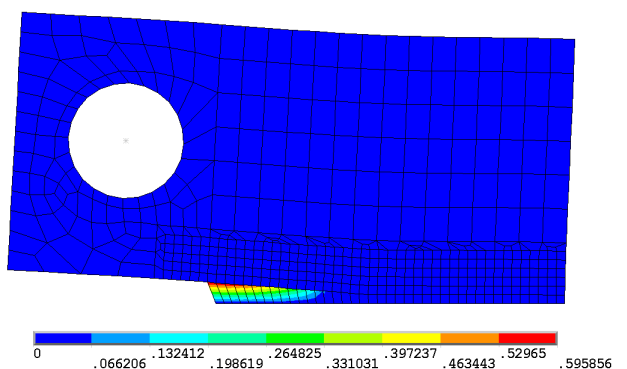


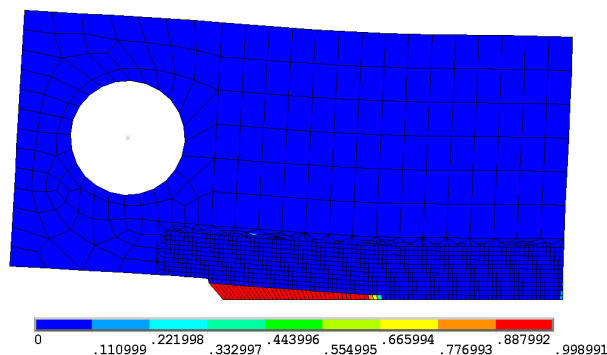
Figure 5.20: Convergence study: Global force-displacement response for three different meshes



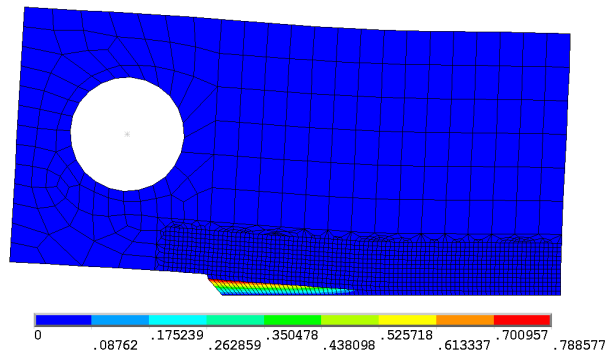
(a) d1, $h = 1\text{mm}$



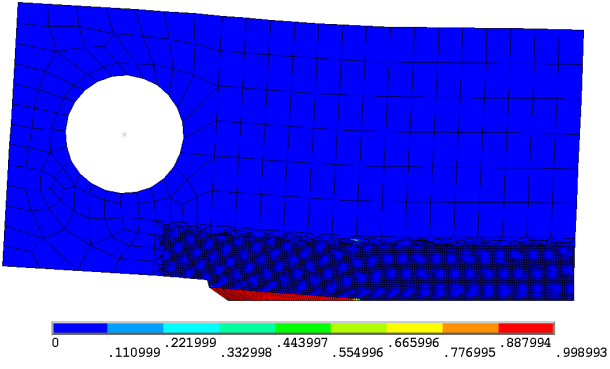
(b) d2, $h = 1\text{mm}$



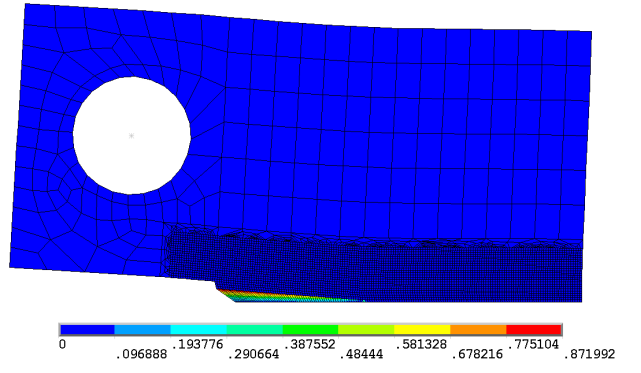
(c) d1, $h = 0.5\text{mm}$



(d) d2, $h = 0.5\text{mm}$



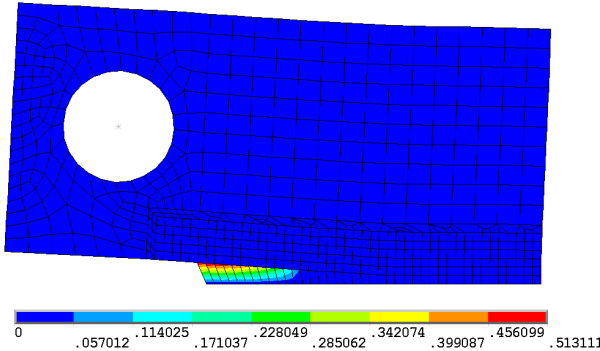
(e) d_1 , $h = 0.25\text{mm}$



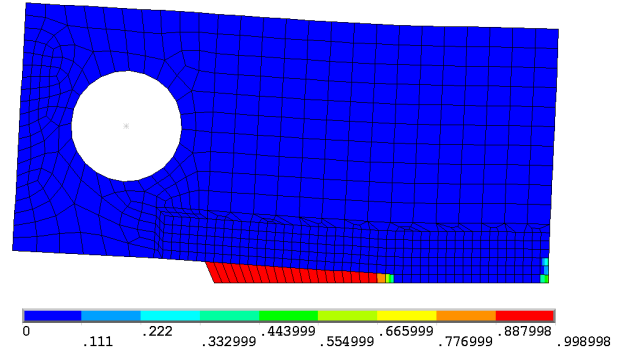
(f) d_2 , $h = 0.25\text{mm}$

Figure 5.21: Damage distributions at the end of loading in longitudinal direction: Damage contour plots d_1 and d_2

Now the transverse direction is kept parallel to the loading direction, and the anisotropic development of damage d_1 and d_2 is analysed. In this case, damage d_2 is the primary damage variable and damage d_1 is dependent on the mesh size. The damage distributions (d_1 and d_2) for loading in transverse direction and force-displacement comparison of longitudinal and transverse loading for $h=1\text{mm}$ discretization are shown in figure (5.22) and (5.23) respectively.



(a) d_1



(b) d_2

Figure 5.22: Damage distributions at the end of loading in transverse direction: Damage contour plots d_1 and d_2 ($h = 1\text{mm}$ discretization)

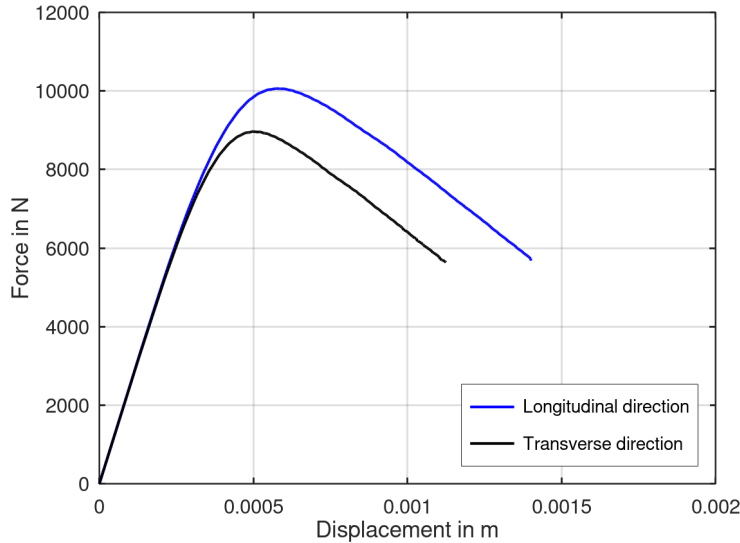


Figure 5.23: Comparison of force-displacement response in longitudinal and transverse direction for $h = 1$ mm discretization

Effect of shear in damage development

To deeply understand the failure of composite materials, the effect of shear on damage initiation and propagation is studied. The effect of shear stress in each failure mechanism is introduced by the modified Hashin's failure criterion (Section (4.3.3)) where α is the shear contribution factor which ranges from 0 to 1. The effect of shear can be studied by varying this shear contribution factor α .

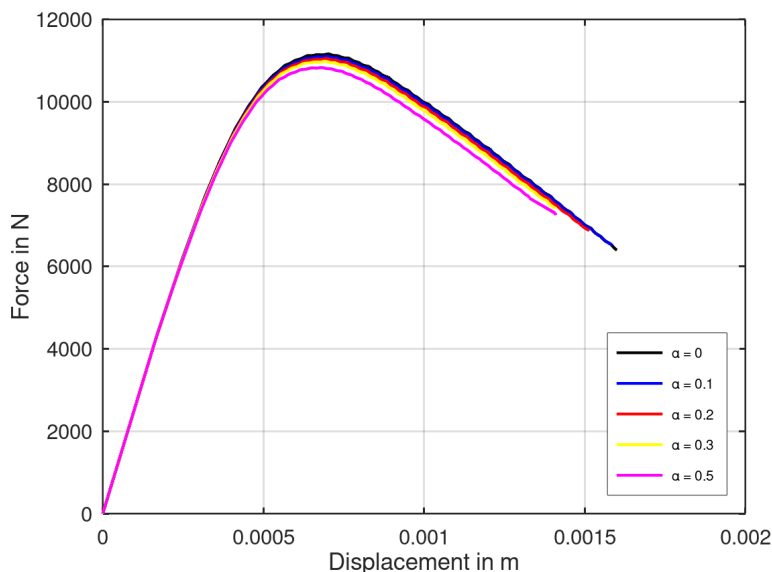


Figure 5.24: Comparison of force-displacement response for different shear coefficient (α) ($h= 1$ mm discretization)

The maximum value of α is chosen to be 0.5 to avoid the damage development only due to shear because the shear strength is low compared to other strengths. The global force-displacement response for different α by loading the CT-Specimen in the longitudinal direction is shown in Figure (5.24). It is evident that by increasing α , the failure index increases, which reduces the maximum load capacity of the CT specimen.

From Figure (5.25), it is clear that the increase in shear contribution has little to no effect in the initiation and distribution of the damage d_1 because the shear stress component (σ_{12}) is very low compared to the stress component (σ_{11}) which is responsible for damage d_1 . However, the shear stress (σ_{12}) affects the damage d_2 because its magnitude is significant compared to the stress component (σ_{22}) which is the only component responsible for damage d_2 in the case of the maximum stress criterion previously employed.

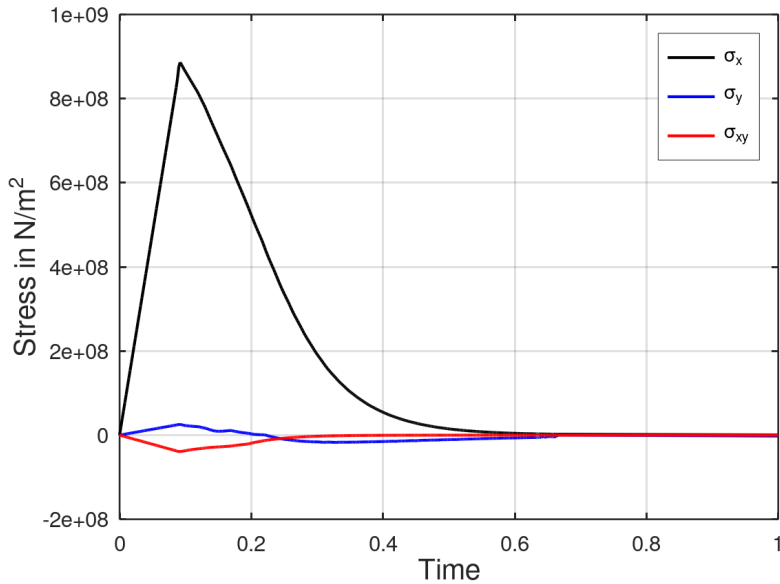


Figure 5.25: Evolution of stress components during longitudinal tensile loading ($h=1\text{mm}$ discretization)

The contour plots of damage d_2 for increasing shear contribution are plotted in Figure (5.26). Compared to no shear effect ($\alpha = 0$), the model with the presence of shear effect has more realistic damage propagation of (d_2), and the width of the damage zone is significantly larger. For the model with shear effect, the width of the damage zone is almost similar in all the cases, but the maximum damage value and the number of elements reaching critical damage value increase with the increase in α .

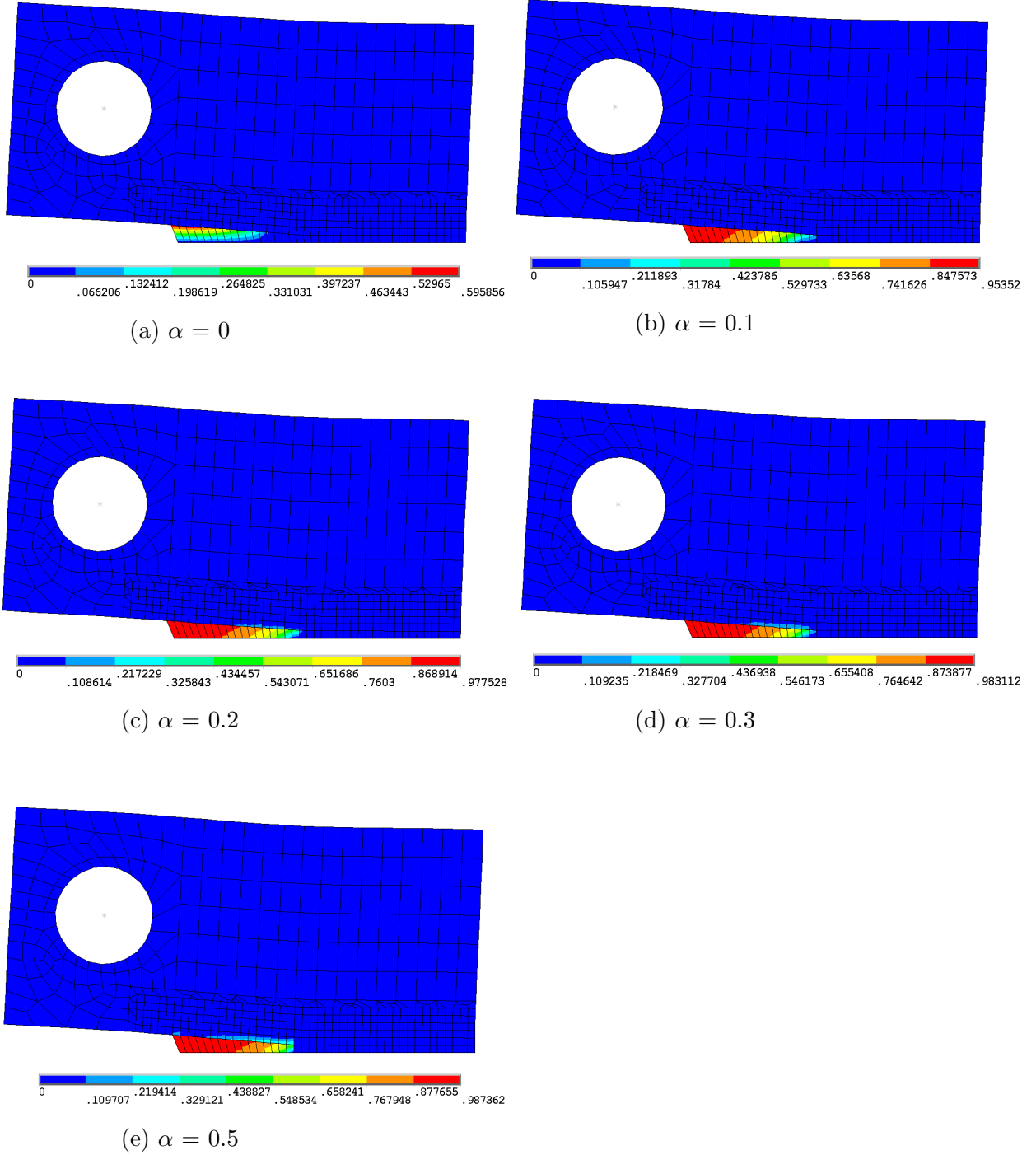


Figure 5.26: Damage distributions at the end of longitudinal loading: Damage contour plots d_2 for different shear co-efficients (α)

In the case of transverse loading, the damage d_2 is unaffected because the magnitude of the shear stress (σ_{12}) is very low compared to the stress (σ_{22}). However, the damage d_1 is affected because the magnitude of the shear stress component (σ_{12}) is similar compared to (σ_{11}).

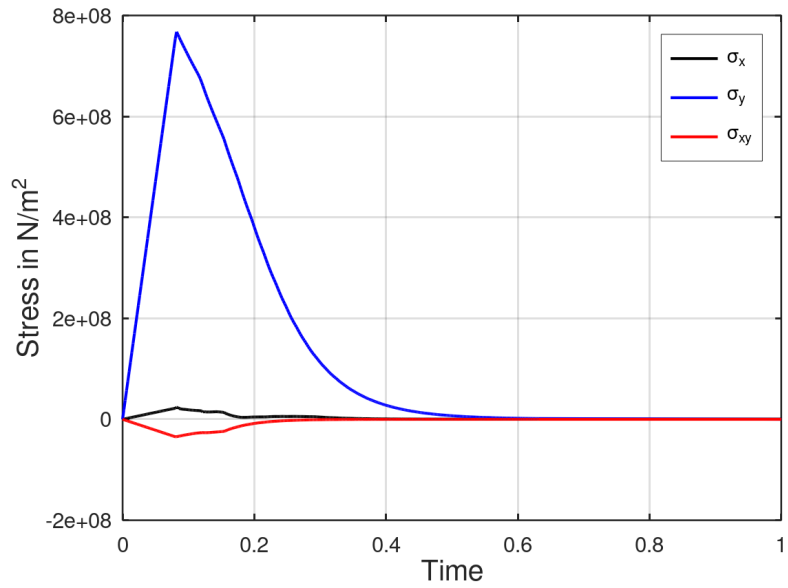


Figure 5.27: Evolution of stress components during transverse tensile loading ($h=1\text{mm}$ discretization)

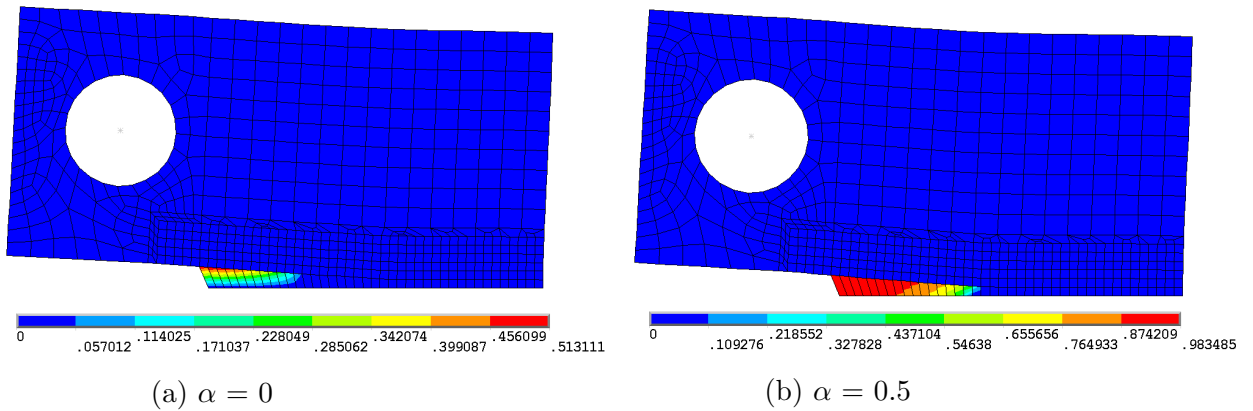


Figure 5.28: Damage distributions at the end of transverse loading: Damage contour plots d_1 for different shear co-efficient (α)

5.3.3 Plate with hole (3D)

This third example demonstrates the model's ability to show the anisotropic damage development for three dimensional (3D) problems. In 3D, three damage variables (d_1 , d_2 and d_3) are employed to represent the anisotropic damage development, i.e., one damage variable for each principal material direction. Because of symmetry, only one-eighth of the specimen has been modelled. The geometry and the appropriate boundary conditions are given in Figure (5.29). Eight node solid elements (SOLID 185) with trilinear interpolations of the displacements and full integration has been used to perform the FE modelling. The thickness was divided into four elements, and a fine mesh has been used in the region closer to the fracture zone shown in the Figure (5.30).

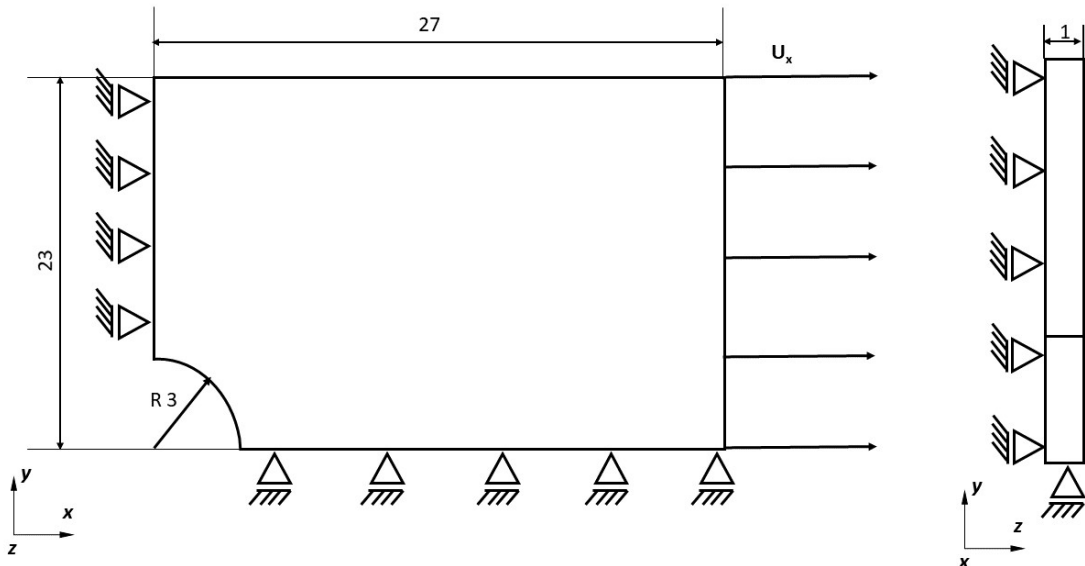


Figure 5.29: Specimen geometry and boundary conditions. Dimensions are given in mm. Displacement controlled loading U_x is applied

The longitudinal direction is kept parallel to the loading direction, and the behaviour of the model is analysed by applying displacement controlled load (U_x) in the longitudinal direction (X-direction). The strength in transverse directions (2 and 3) are large enough for the damage variables d_2 and d_3 not to initiate when a longitudinal tensile load is applied. So to demonstrate the model's capability to show anisotropic damage development the transverse strength has been reduced to 300 MPa (For both tension and compression). The material properties considered for 3D damage model are given in the Table. (5.3). The maximum stress criterion (See Section(4.3.2)) has been used to predict the damage initiation in the three principal material directions.

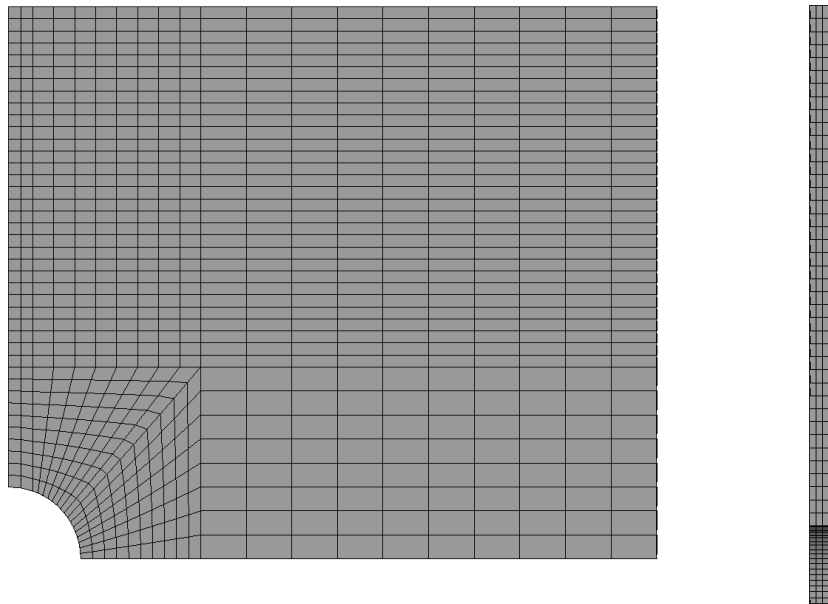


Figure 5.30: Finite element discretization used for 3D damage study

Symbol	Material Parameter	Value
E_{11}	Modulus in longitudinal (1) direction	55.8 GPa
$E_{22} = E_{33}$	Modulus in transverse (2 and 3) directions	54.9 GPa
$\nu_{12} = \nu_{13}$	Poisson's ratio	0.043
$G_{12} = G_{23} = G_{13}$	Shear modulus	4.2 GPa
X_t	Tensile strength in longitudinal (1) direction	910.1 MPa
X_c	Compressive strength in longitudinal (1) direction	-710.2 MPa
Y_t	Tensile strength in (2 and 3) directions	300 MPa
Y_c	Compressive strength in (2 and 3) directions	-300 MPa
S_{12}	In-plane strength	131 MPa
G_f^{lt}	Tensile fracture energy along longitudinal (1) direction	125 KJ/m ²
G_f^{lc}	Compressive fracture energy along longitudinal (1) direction	250 KJ/m ²
G_f^{tt}	Tensile fracture energy along (2 and 3) directions	95 KJ/m ²
G_f^{tc}	Compressive fracture energy along (2 and 3) directions	254 KJ/m ²

Table 5.3: Material parameters (3D Damage model)

The global force-displacement response has been plotted for this longitudinal tensile loading in Figure (5.31). The response is similar to the longitudinal loading in the notched tensile specimen, being characterized by a linear regime followed by a gradual drop of the load because of the softening. The softening is observed to initiate when the damage happens in critical number of elements in the fracture zone.

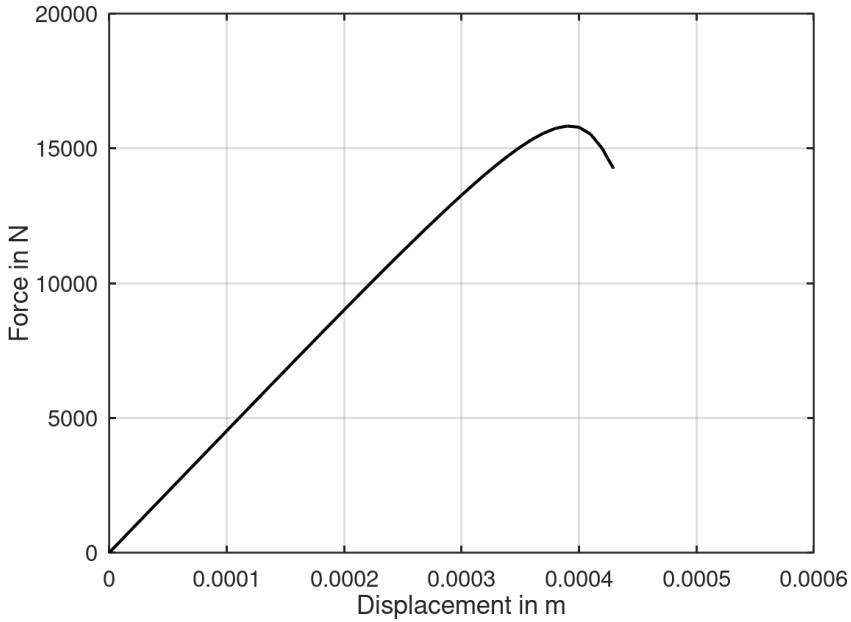
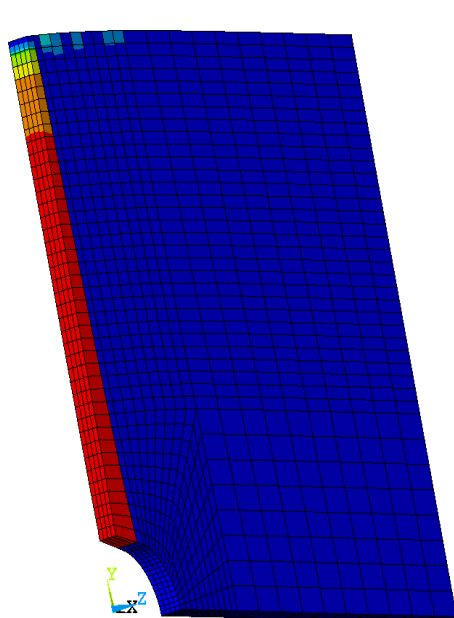


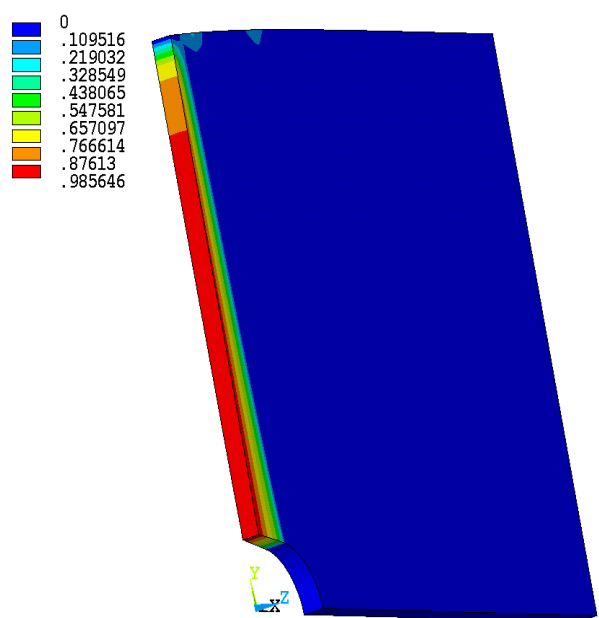
Figure 5.31: Global force-displacement response for the longitudinal tensile loading

The damage distribution (d_1 , d_2 and d_3) at the end of the tensile loading is shown in the Figure (5.32). In order to get a good visualization and understanding both element and nodal solution values of the damage are plotted. The initiation and evolution of damage d_1 is caused by the normal stress component σ_{11} in the longitudinal direction. The damage d_1 initiates at the tip of the blunt notch and then propagates perpendicular to the loading direction.

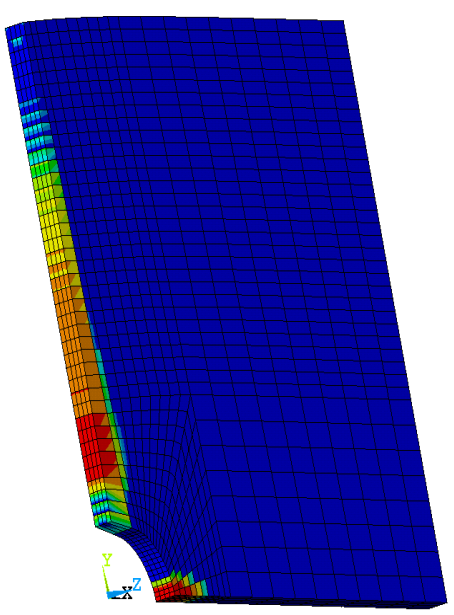
From Figures (5.32c) and (5.32d) it is evident that the damage happens at two separate regions, i) perpendicular to the loading direction where damage d_1 already propagated ii) right at the blunt notch at the bottom edge of the plate. It has been observed that the damage d_2 in the region (i) happens because of tension in the transverse direction, and in the region (ii) the damage is caused by the compression in the transverse direction. The propagation of damage d_3 is caused by the normal stress component σ_{33} in the thickness direction. The damage d_2 and d_3 has much lesser influence on the strength of the specimen compared to the damage d_1 during longitudinal tensile loading.



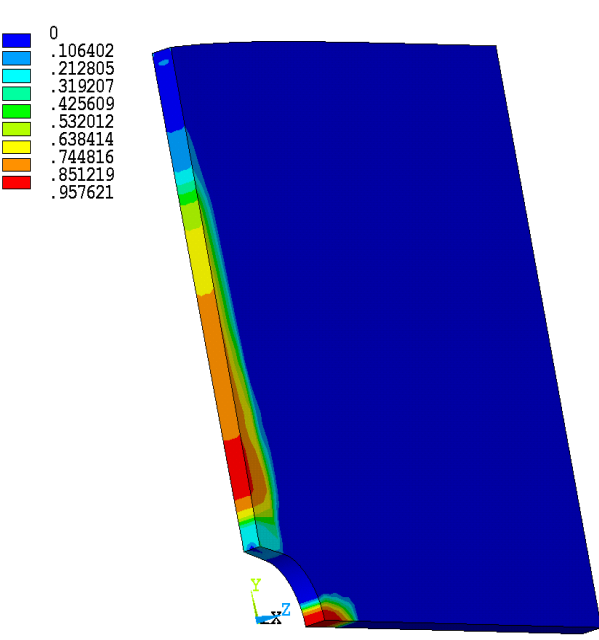
(a) Damage d_1 - Element solution



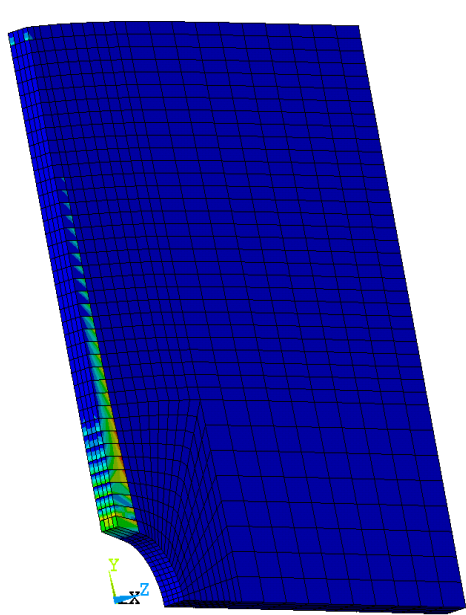
(b) Damage d_1 - Nodal solution



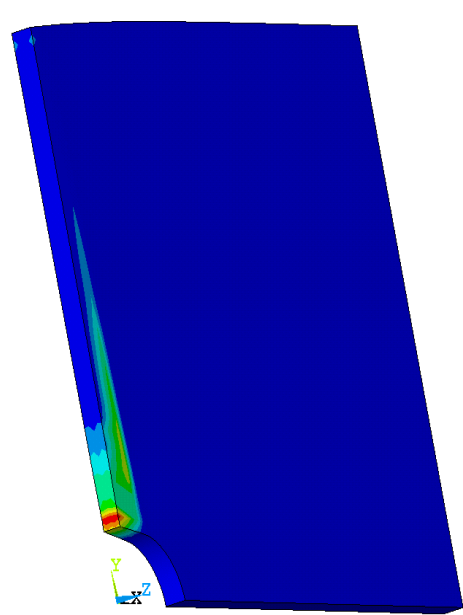
(c) Damage d_2 - Element solution



(d) Damage d_2 - Nodal solution



(e) Damage d_3 - Element solution



(f) Damage d_3 - Nodal solution

Figure 5.32: Contour plots of the damage distribution d_1 , d_2 and d_3 at the end of longitudinal tensile loading

These damage contour plots clearly indicate that the developed 3D model has the ability to show not only the damage development in three principal material directions but also both tension and compression damage happening simultaneously in a specimen when a load is applied.

Chapter 6

Summary and Conclusion

The main objective of this work is to develop progressive damage models which can clearly describe the damage mechanism in orthotropic composite materials when subject to various loading conditions. The models are developed using the framework of continuum damage mechanics (CDM) which uses internal state variables to describes the evolution of damage in a material using evolution laws. A second-order orthotropic damage tensor is employed to show the anisotropic damage development where the eigen values of the damage tensor represents damage in each principal material direction. A key issue in damage modelling is the convergence issue that arise due to the mesh dependant behaviour of the strain-softening models. To reduce the mesh sensitivity, fracture energy regularization technique has been employed which ensures the objectivity of the model by adjusting dissipated energy to each finite element. At first the damage models (both 2D/Plane-stress and 3D cases) are implemented in OCTAVE and tested using constitutive driver routines for simple loading cases to verify the numerical implementation i.e., to ensure the convergence of the model with the derived algorithmic tangent stiffness, and to understand the behaviour of the material at integration point level i.e., damage-evolution and strain-softening. During the integration point studies it has been observed that the failure criteria which uses strain to predict the damage initiation causes convergence issues when damage evolves without the presence of stress in the given material direction i.e., when transverse strength is very low and an uniaxial tension is applied in longitudinal direction. So the damage models implemented as user-defined material routines (USERMAT) in ANSYS uses stress-based damage initiation criteria

The user-defined material routines (USERMAT) are tested using a finite element of unit length in ANSYS in order to compare against the results from OCTAVE implementation. Once verified, representative structural examples (both 2D and 3D) are used to test the damage models in ANSYS to see how they predict the initiation and evolution of damage under various circumstances. Finite elements of varying sizes are used in the area prone to damage to analyse the mesh sensi-

tivity of the damage models. It has been observed that the regularization scheme used significantly improves the global response but it does not fully alleviate the mesh dependency problems which arise due to strain-softening. Therefore a drop in maximum load is observed in the global force-displacement response when the mesh is refined. Different damage initiation criteria has been employed to see how the damage initiation and failure indices affect the model. It has been observed that the inclusion of shear effect naturally reduces the maximum load capacity because of the increase in failure index for the same load. In some cases the shear effect improves the damage propagation and distribution when the magnitude of shear stress is significant compared to the normal stresses. Finally the implemented damage models employing exponential damage evolution laws have the ability to show the anisotropic damage development with the help of a second-order damage tensor in both 2D and 3D cases and the strain-softening which results due to the stiffness degradation. This work provides a better understanding of the numerical implementation of anisotropic damage models which can predict the damage behaviour of complex composite materials.

The following changes and developments can be made in future to make this anisotropic damage model an excellent tool to analyze the complex damage phenomena in composite-materials used in real-life applications

- By incorporating complex failure criteria like Linde's failure criteria, Hashins quadratic failure criteria etc., the damage initiation and propagation can be predicted more accurately because of the inclusion of shear effects and quadratic terms.
- From section (5.3.2) (CT-Specimen) it is evident that when most of the distorted elements reaches a critical value the simulation terminates. This has been the case in most of the work done before. But in very few works an option called element deletion (Available in the FEM software Abaqus) is employed to delete a particular failed element when the damage reaches a critical threshold value. This option can be included in the future to avoid the premature termination of analysis and the whole crack propagation in the case of CT specimen can be simulated.
- Non-local gradient-enhanced damage formulations can be incorporated into the anisotropic damage models to eliminate the mesh dependency problems encountered in this work. These non-local models uses weighted volume averages of the state variables to create spatial interactions which induces smoothing effect on the deformation and damage. Gradient enhanced formulations uses higher-order deformation gradients of internal variables to create spatial discretization thereby eliminating the mesh dependency

Appendix

A.1 Elastic stiffness matrix of the damaged material

A.1.1 Plane stress (2D)

The elastic stiffness matrix of the damage material for transversely isotropic material has the form

$$\mathbb{C}(D) = \frac{1}{D} \begin{bmatrix} C_{11}(1-d_1) & C_{12}(1-d_1)(1-d_2) & 0 \\ C_{21}(1-d_2)(1-d_1) & C_{22}(1-d_2) & 0 \\ 0 & 0 & D(1-d_3)G_{12} \end{bmatrix}$$

where $D = 1 - (1-d_1)(1-d_2)\nu_{12}\nu_{21}$ and $d_3 = 1 - (1-d_1)(1-d_2)$

A.1.2 3D

The elastic stiffness matrix of the damage material for orthotropic material has the form

$$\mathbb{C}(D) = \begin{bmatrix} C_{11}^d & C_{12}^d & C_{13}^d & 0 & 0 & 0 \\ C_{21}^d & C_{22}^d & C_{23}^d & 0 & 0 & 0 \\ C_{31}^d & C_{32}^d & C_{33}^d & 0 & 0 & 0 \\ 0 & 0 & 0 & C_{44}^d & 0 & 0 \\ 0 & 0 & 0 & 0 & C_{55}^d & 0 \\ 0 & 0 & 0 & 0 & 0 & C_{66}^d \end{bmatrix}$$

where $C_{ij}^d = (1 - d_i)(1 - d_j)$, $i, j = 1, 2, 3$

$$C_{44}^d = (1 - d_1)(1 - d_2),$$

$$C_{55}^d = (1 - d_1)(1 - d_3),$$

$$C_{66}^d = (1 - d_2)(1 - d_3)$$